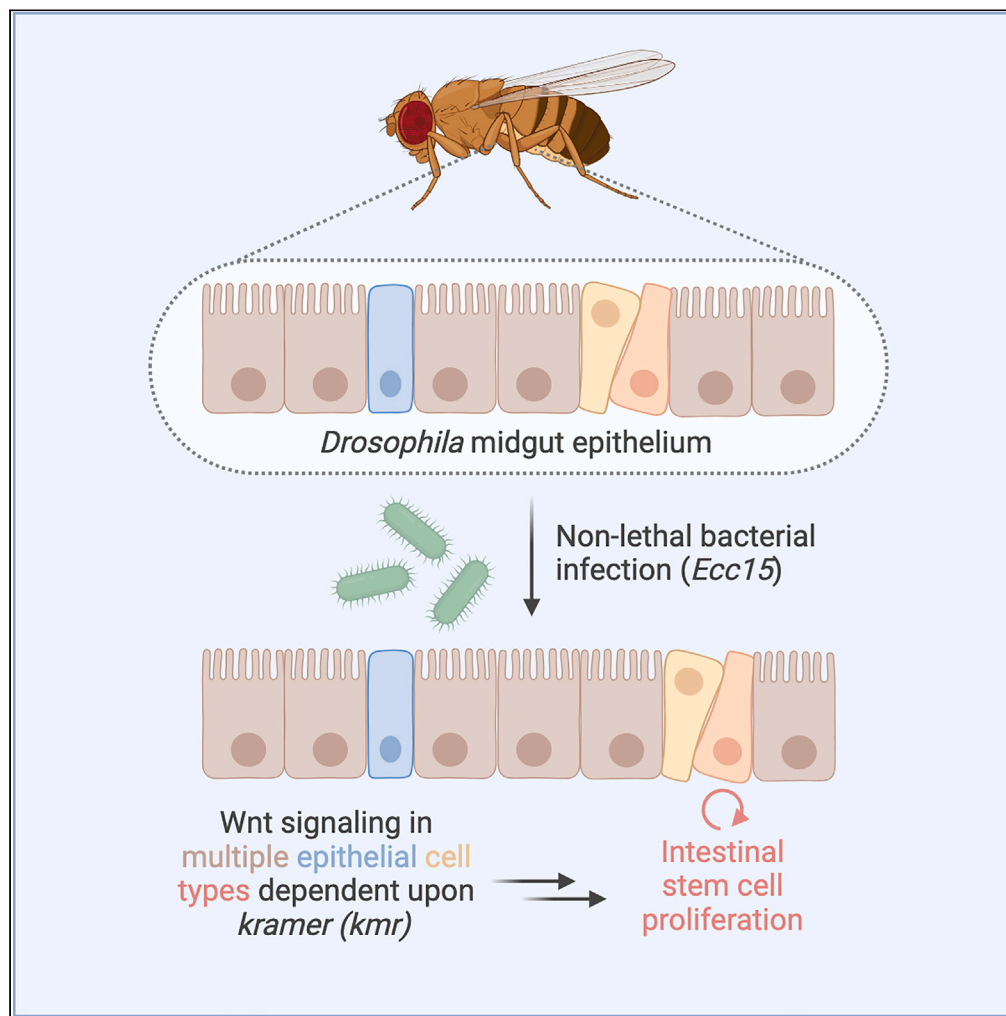


## Article

Wnt/ $\beta$ -catenin signaling within multiple cell types dependent upon *kramer* regulates *Drosophila* intestinal stem cell proliferation

Hongyan Sun,  
Adnan Shami  
Shah, Din-Chi  
Chiu, Alessandro  
Bonfini, Nicolas  
Buchon, Jeremy M.  
Baskin

jeremy.baskin@cornell.edu

**Highlights**

*Kramer* is a physiological regulator of Wnt/ $\beta$ -catenin signaling in the fly midgut

Wnt signaling in several gut epithelial cell types promotes stem cell proliferation

*Kramer* acts by antagonizing the Cullin-3 E3 ligase adaptor *kelch*

Enteroendocrine cells play non-autonomous roles in midgut stem cell proliferation

Sun et al., iScience 27, 110113  
June 21, 2024 © 2024 The  
Author(s). Published by Elsevier  
Inc.  
<https://doi.org/10.1016/j.isci.2024.110113>

## Article

Wnt/ $\beta$ -catenin signaling within multiple cell types dependent upon *kramer* regulates *Drosophila* intestinal stem cell proliferation

Hongyan Sun,<sup>1</sup> Adnan Shami Shah,<sup>1,2</sup> Din-Chi Chiu,<sup>1,2</sup> Alessandro Bonfani,<sup>3,4,5</sup> Nicolas Buchon,<sup>3</sup> and Jeremy M. Baskin<sup>1,2,6,\*</sup>

## SUMMARY

The gut epithelium is subject to constant renewal, a process reliant upon intestinal stem cell (ISC) proliferation that is driven by Wnt/ $\beta$ -catenin signaling. Despite the importance of Wnt signaling within ISCs, the relevance of Wnt signaling within other gut cell types and the underlying mechanisms that modulate Wnt signaling in these contexts remain incompletely understood. Using challenge of the *Drosophila* midgut with a non-lethal enteric pathogen, we examine the cellular determinants of ISC proliferation, harnessing *kramer*, a recently identified regulator of Wnt signaling pathways, as a mechanistic tool. We find that Wnt signaling within Prospero-positive cells supports ISC proliferation and that *kramer* regulates Wnt signaling in this context by antagonizing *kelch*, a Cullin-3 E3 ligase adaptor that mediates Dishevelled poly-ubiquitination. This work establishes *kramer* as a physiological regulator of Wnt/ $\beta$ -catenin signaling *in vivo* and suggests enteroendocrine cells as a new cell type that regulates ISC proliferation via Wnt/ $\beta$ -catenin signaling.

## INTRODUCTION

The adult *Drosophila melanogaster* intestine is a powerful model to study stem cell proliferation.<sup>1–5</sup> The fly gut has many important physiological functions, most notably nutrient absorption, acting as a physical barrier, and providing immunity to enteric pathogens and chemical insults.<sup>1,2</sup> A conserved hallmark of the gut is the dynamic nature of its architecture.<sup>3–5</sup> The *Drosophila* midgut is the largest and central portion of the intestines, and it is analogous to the mammalian small intestine in function and, to some extent, cellular architecture and composition.<sup>6</sup>

The signature feature of the midgut is its epithelium, a single cell layer acting as a barrier to separate the lumen from internal tissues. In *Drosophila*, the midgut epithelium comprises four principal cell types. Intestinal stem cells (ISCs) can self-renew and also give rise to progenitor cells termed enteroblasts (EBs), which in turn can fully differentiate into enterocytes (ECs) that comprise the bulk of the epithelium. The specification of the fourth cell type, enteroendocrine cells (EEs), has not been fully elucidated, despite the importance of these cells in mediating important paracrine signaling events.<sup>7–10</sup> EBs have been proposed to differentiate into EEs;<sup>11,12</sup> however, recent studies demonstrated that ISCs, when Prospero-positive, divide into a distinct progenitor type termed pre-EEs, which subsequently differentiate into EEs.<sup>13–15</sup> Disruption of ISC function can lead to either excessive proliferation or precocious differentiation, often resulting in disease.<sup>8,9,16,17</sup> Therefore, a detailed understanding of the pathways and mechanisms regulating ISC proliferation is an important long-term goal with therapeutic implications.

Numerous studies have shown that Wnt/ $\beta$ -catenin signaling, a morphogen signaling pathway that is highly conserved in animals, promotes ISC proliferation and differentiation under both physiological conditions and upon challenges such as enteric infection or chemical insults, both of which can damage the gut epithelium. More broadly, Wnt/ $\beta$ -catenin signaling, also known as canonical Wnt signaling, controls diverse cellular processes during animal development and homeostasis, including stem cell maintenance, cell fate specification, neural patterning, spindle orientation, cell migration, cell polarity, and gap junction communication.<sup>18–22</sup> Dysregulation of canonical Wnt signaling caused by mutations of core components of this pathway is frequently linked to birth defects and many types of cancer.<sup>23–26</sup> During tissue development and homeostasis, canonical Wnt signaling is thought to be the main pathway for regulating ISC proliferation and self-renewal, which drives massive renewal processes of intestinal epithelial cells.<sup>13–15</sup>

<sup>1</sup>Weill Institute for Cell & Molecular Biology, Cornell University, Ithaca, NY 14853, USA

<sup>2</sup>Department of Chemistry & Chemical Biology, Cornell University, Ithaca, NY 14853, USA

<sup>3</sup>Cornell Institute of Host Microbe Interactions and Disease, Department of Entomology, Cornell University, Ithaca, NY 14853, USA

<sup>4</sup>Zhejiang University-University of Edinburgh Institute, Zhejiang University School of Medicine, Zhejiang University, Haining 314400, P.R. China

<sup>5</sup>Edinburgh Medical School: Biomedical Sciences, College of Medicine and Veterinary Medicine, The University of Edinburgh, Edinburgh, UK

<sup>6</sup>Lead contact

\*Correspondence: [jeremy.baskin@cornell.edu](mailto:jeremy.baskin@cornell.edu)

<https://doi.org/10.1016/j.isci.2024.110113>



Despite the fundamental importance of Wnt signaling in regulating ISC proliferation and subsequent tissue renewal in the gut epithelium,<sup>13–15,27</sup> our understanding of how Wnt signaling in different cell types within the gut contributes to these effects on ISCs is still rudimentary. Furthermore, recent studies have elucidated roles for  $\beta$ -catenin-independent, or non-canonical Wnt signaling pathways, which share some upstream components in the Wnt-receiving cell but do not activate  $\beta$ -catenin-dependent gene expression, in regulating ISC proliferation in the *Drosophila* midgut.<sup>28</sup> Thus, knowledge of which cell types exhibit canonical and non-canonical Wnt signaling that collectively contribute to ISC proliferation and thus tissue maintenance in the midgut are major fundamental and unanswered questions.

A key shared player in all Wnt signaling pathways is Disheveled (Dsh/DVL), which is recruited to the plasma membrane upon activation of Wnt receptors and co-receptors from the Frizzled and low density lipoprotein receptor-related protein (LRP) families. Such recruitment catalyzes the disassembly of a multiprotein complex that facilitates proteasomal degradation of  $\beta$ -catenin, enabling its accumulation and subsequent translocation to the nucleus to activate T-cell factor/lymphoid enhancer factor (TCF/LEF)-dependent gene expression in the canonical pathway.<sup>18,19</sup> Dsh recruitment to the plasma membrane also activates planar cell polarity (PCP) and other non-canonical Wnt pathways, including the Wnt/ $\text{Ca}^{2+}$  pathway, by activation of Frizzled receptors.<sup>20</sup> Thus, regulation of Dsh levels, which occurs via the ubiquitin-proteasome system and involves the action of several distinct E3 ubiquitin ligases,<sup>29–35</sup> is a key control point in all Wnt signaling pathways.

Notably, we previously discovered that a mammalian multi-subunit phosphoinositide-binding protein, pleckstrin homology domain-containing family A number 4 (PLEKHA4), promotes both Wnt/ $\beta$ -catenin and non-canonical Wnt signaling in human cell lines by antagonizing DVL polyubiquitination by the Cullin-3 (CUL3)-Kelch-like protein 12 (KLHL12) E3 ubiquitin ligase.<sup>22</sup> We found as well that Wnt/ $\beta$ -catenin signaling and subsequent cell proliferation in mouse models of melanoma were dependent upon PLEKHA4 expression.<sup>23</sup> In *Drosophila*, knockout of the closest fly ortholog of PLEKHA4, *kramer* (*kmr*), impairs PCP in the adult wing, larval wing imaginal disc, and pupal wing disc epithelium.<sup>22</sup> The absence of any discernable defects in canonical Wnt signaling in *kmr* knockout flies led us to question whether *kmr* indeed controlled Wnt/ $\beta$ -catenin signaling in this organism. We proposed that the extent to which PLEKHA4/*kmr* loss affected canonical or non-canonical Wnt pathways might depend on cellular and tissue contexts, where expression of other factors downstream of DVL/Dsh might govern how tuning of DVL/Dsh levels would differentially affect outcomes from these pathways.

To test this prediction, we investigated the role of *kmr* in controlling ISC proliferation in the *Drosophila* midgut, a physiological process dependent upon canonical Wnt signaling and recently linked to non-canonical Wnt signaling pathways as well.<sup>28</sup> Our experimental model involved challenge of adult flies with *Erwinia carotovora carotovora* 15 (*Ecc15*), a gram-negative bacterium that produces non-lethal infection, to damage the midgut epithelium and induce repair pathways dependent upon ISC proliferation.<sup>1,24</sup> Here, we performed global knockout and cell type-specific knockdown of *kmr* and compared effects on tissue pathophysiology to those induced by knockdown of other established components of Wnt signaling pathways. As such, our study accomplished several goals. First, we establish roles for *kmr* in controlling canonical Wnt signaling in *Drosophila*. Second, we use *kmr* as a tool to elucidate roles for canonical and non-canonical Wnt signaling within different cell types in the *Drosophila* midgut. Our studies reveal not only that *kmr*-dependent canonical Wnt signaling controls ISC proliferation in the midgut but that such signaling occurs in several cell types, including Prospero-positive cells, suggesting that EEs, which our studies support derive from pre-EE progenitors, may play an unexpectedly important role in these processes.

## RESULTS

### Expression pattern of *kramer* in the *Drosophila* midgut overlaps with zones of Wnt signaling activation

The *Drosophila* midgut comprises five major regions termed R1–R5, from anterior to posterior, based on anatomical, morphometric, and histological characterization.<sup>25,26</sup> We began our study by investigating levels of Wnt signaling and *kmr* expression in these five regions (Figure S1A). Consistent with previous studies, *frizzled 3* (*fz3*), a direct target gene of canonical Wnt signaling, was expressed in gradients at the boundaries of the intestinal regions with highest expression in R1 and R5 and weaker expression in R2, R3, and R4 by examination of an *fz3-RFP* transgene (Figures S1A and S1B).<sup>26,36</sup> To examine *kramer* (*kmr*) expression, we examined the fly gut-seq dataset, which contains comprehensive RNA-seq data from each of these regions.<sup>12</sup> Interestingly, *kmr* expression was highest within R1 and R5, with moderate expression in R2 and R4, a pattern that aligns with *fz3* expression (Figure S1C).<sup>12</sup> Coupled with our previous finding that the human ortholog of *kmr*, PLEKHA4, promotes Wnt/ $\beta$ -catenin signaling,<sup>22</sup> we postulated that the overlapping expression patterns of *kmr* and *fz3* in the *Drosophila* midgut supports a potential role for *kmr* in regulating Wnt signaling in the fly intestine. These findings prompted us to further investigate the potential functions of *kmr* in regulating Wnt signaling *in vivo* in the *Drosophila* midgut.

### *Kmr* is required to activate canonical Wnt signaling in the fly midgut

To investigate whether *kmr* regulates canonical Wnt signaling *in vivo*, we subjected wild type (WT), *kmr* knockout (KO), and tissue-specific *kmr* knockdown fly strains to infection with a non-lethal dose of *E. carotovora carotovora* 15 (*Ecc15*), a gram-negative bacterium that damages differentiated ECs, followed by recovery, which features a regenerative response.<sup>1</sup> First, we examined effects on *fz3* expression in the midgut in two global KO strains generated via CRISPR/Cas9-mediated mutagenesis, *kmr*<sup>1</sup> and *kmr*<sup>2</sup>, which contain 1 bp and 2 bp deletions to create frameshift mutations starting at the 88<sup>th</sup> and 89<sup>th</sup> bases, respectively.<sup>22</sup> Because canonical Wnt signaling exhibits high activity in the R5 (posterior) region,<sup>13</sup> we performed our analysis primarily in this region, unless otherwise indicated. In both unchallenged (UC) and *Ecc15*-infected groups, *Fz3-RFP* expression was significantly lower in both *kmr* KO strains compared to control flies (Figures 1A–1D).

We then performed cell type-specific *kmr* knockdown using the *Gal4/UAS-GFP* system. In ISCs and EBs, as revealed by *esg-Gal4*, *UAS-GFP*, *tub-Gal80<sup>ts</sup>* (*esg<sup>ts</sup>*), *kmr* knockdown downregulated the expression of *fz3-RFP* (Figures 1E, 1F, and 1K). Analogously, we found that *kmr* knockdown in ECs, driven by *myo<sup>ts</sup>-Gal4*, *UAS-GFP*, *tub-Gal80<sup>ts</sup>* (*myo<sup>ts</sup>*), attenuated *fz3-RFP* expression both inside the compartments

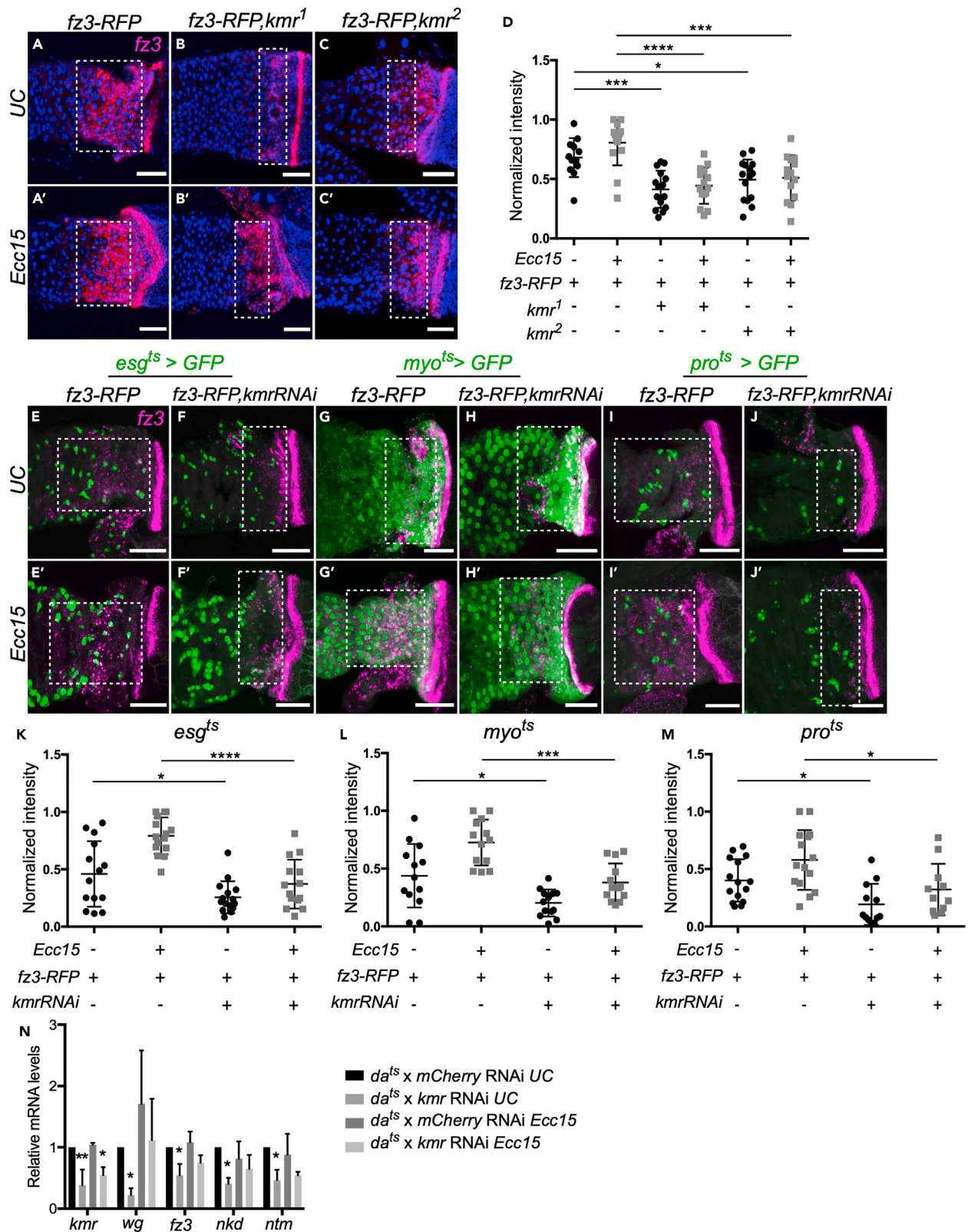


### Figure 1. Loss of *kramer* attenuates *frizzled3* expression in the posterior midgut

(A–D) Two *kmr* knockout strains (*kmr*<sup>1</sup> and *kmr*<sup>2</sup>) exhibit decreased *fz3-RFP* expression in the posterior midgut relative to WT both in unchallenged (UC) conditions and following non-lethal infection with *Erwinia carotovora carotovora* 15 (*Ecc15*). Shown in (A–C) are representative confocal micrographs (z-projection images), with quantification (white box area) for each genotype shown in (D).

(E–M) Cell type-specific RNAi-mediated *kmr* knockdown decreases *fz3-RFP* expression in four different midgut cell types: intestinal stem cells (ISCs) and enteroblasts (EBs) (*esg*<sup>ts</sup>>*GFP*), enterocytes (ECs, *myo*<sup>ts</sup>>*GFP*), and enteroendocrine cells (EEs, *pro*<sup>ts</sup>>*GFP*). Shown in (E–J) are high-magnification images of the midgut-hindgut boundary, which exhibits high *fz3-RFP* expression.

(N) Ubiquitous expression marker *Daughterless-Gal4; Tub-Gal80*<sup>ts</sup> (*da*<sup>ts</sup>) was used for global *kmr* knockdown, and *mCherry* RNAi was used as a negative control. Expression of *kmr* RNAi in the midgut led to a decrease in the mRNA expression levels of Wnt signaling target genes and components, including *wg*, *fz3*, *naked* (*nkd*), and *notum* (*ntm*). The mRNA levels of all these genes were reduced in the midgut, as measured by RT-qPCR. The values represent the fold change relative to the unchallenged control. Green: GFP (RNAi); Magenta: Fz3-RFP (anti-mCherry antibody). Quantification (white boxed area) of Fz3-RFP expression is shown in (K–M). Data points represent individual midguts (black circles, UC; gray squares, *Ecc15*), lines represents mean, and error bars denote standard deviation. Statistical significance was determined using one-way ANOVA with Tukey post-hoc test. \*\*\*\*, *p* < 0.0001; \*\*\*, *p* < 0.001; \*\*, *p* < 0.01; \*, *p* < 0.05; ns: not significant; *n* = 11–15. Scale bars: 40 μm.

and at boundaries (Figures 1G, 1H, and 1L). Finally, *kmr* knockdown in EEs, driven by *pro*<sup>ts</sup>-*Gal4*, *UAS-GFP*, *tub-Gal80*<sup>ts</sup> (*pro*<sup>ts</sup>), decreased *fz3-RFP* expression (Figures 1I, 1J, and 1M). Furthermore, we assessed the impact of *kmr* on the regulation of Wnt target genes. Global *kmr* knockdown in the midgut, confirmed by RT-qPCR, resulted in downregulation of the expression of *wg*, *fz3*, *naked*, and *notum* in both unchallenged and *Ecc15*-challenged groups (Figure 1N). These results show that *kmr* knockdown globally and in each major midgut cell type negatively affected canonical Wnt signaling elicited by *Ecc15* challenge, consistent with its role as a positive regulator of Wnt/β-catenin signaling in mammalian cells, though it is noted that such RT-qPCR analysis on whole tissues cannot establish the cell autonomous nature of such signaling.

### Loss of *kmr* attenuates stem cell proliferation in the midgut

We next sought to establish the role of *kmr* in governing ISC proliferation using *Ecc15* infection followed by recovery. As a primary readout, we imaged and quantified the number of dividing cells positive for phosphorylated histone 3 at serine 10 (pH3<sup>+</sup>).<sup>1,12,26</sup> Both global *kmr* KO strains exhibited a decreased number of pH3<sup>+</sup> stem cells relative to WT control (Figures 2A–2C and 2E). To further confirm the specificity of the effects to *kmr* KO in the two global knockout strains, we generated a *kmr*<sup>1</sup>/*kmr*<sup>2</sup> compound heterozygote and found that it displayed an identical decrease in number of pH3<sup>+</sup> cells (Figures 2D and 2E).

To confirm the effect of *kmr* loss on stem cell proliferation, we also used an inducible flip-out system under the control of *esg-Gal4* (*esg*<sup>F/O</sup>), which results in GFP expression in ISCs, EBs, and their progeny following induction by temperature switch.<sup>5,37,38</sup> Using this system, we found that RNAi-mediated *kmr* knockdown decreased stem cell proliferation (Figures 2F–2H), as assessed by quantification of both GFP<sup>+</sup> and pH3<sup>+</sup> cells. These results confirm that *kmr* promotes ISC proliferation in the midgut.

### Cell type-specific *kmr* knockdown reveals role for Prospero<sup>+</sup> cells in controlling ISC proliferation

To establish the cell type(s) in which *kmr* expression most strongly affects stem cell proliferation, we tested the effects of *kmr* knockdown in ISCs/EBs, ECs, and EEs separately. We found that *kmr* knockdown in ISCs and EBs decreased the number of pH3<sup>+</sup> progenitor cells relative to WT controls, with significant differences observed in the *Ecc15*-challenged groups (Figures 3A, 3B, 3G, S2A, S2B, and S3A). Previous studies have demonstrated that Wnt signaling in ISCs is necessary to drive ISC proliferation, but its role in EBs was less clear.<sup>38</sup> To knock down *kmr* separately in ISC and EBs via RNAi, we employed the cell type-specific drivers *esg-Gal4*, *UAS-eGFP*; *Su(H)-Gal80*, *tub-Gal80*<sup>ts</sup> (*esg::Su(H)*<sup>ts</sup>), and *Su(H)*<sup>ts</sup>-*Gal4*; *UAS-GFP* (*Su(H)*<sup>ts</sup>). Whereas *kmr* knockdown in ISCs significantly reduced the number of pH3<sup>+</sup> cells in *Ecc15*-challenged flies (Figures S4A–S4C), we did not observe a decrease in pH3<sup>+</sup> cells upon *kmr* knockdown in EBs (Figures S4D–S4F).

Knockdown of *kmr* in EC cells (Figures 3C, 3D, 3H, S2C, S2D, and S3B), in EE cells (Figures 3E, 3F, 3I, S2E, S2F, and S3C), and in visceral muscle (Figure S3D) all led to significant decreases in pH3<sup>+</sup> cells in *Ecc15*-challenged flies and also modest reductions in pH3<sup>+</sup> cells in unchallenged flies, relative to negative control (*mCherry*) RNAi. Importantly, knockdown of *kmr* in a tissue outside the midgut, the fat body, using an *lpp*<sup>ts</sup>-*Gal4* (*lpp*<sup>ts</sup>) did not cause a reduction of pH3<sup>+</sup> cells in the midgut (Figure S3E). This result underscores the specificity of our findings that *kmr* knockdown in several different midgut cell types causes proliferation defects in the midgut. To assess whether increased cell death could explain the reduction in pH3<sup>+</sup> cells caused by *kmr* knockdown, we immunostained midguts for cleaved caspase-3 but found no evidence for an increase in this marker (Figure S5). Instead, these studies revealed that *kmr* knockdown in ISCs/EBs and EEs upon *Ecc15* challenge caused a reduction in cleaved caspase-3 signal (Figures S5A, S5B, S5E–S5G, and S5I) and *kmr* knockdown in ECs led to no change (Figures S5C, S5D and S5H), indicating that the reduction in pH3<sup>+</sup> cells is not attributable to an increase in cell death. Previous studies have shown that inactivation of canonical Wnt signaling in ECs negatively impacts stem cell proliferation.<sup>36,39,40</sup> Our results here demonstrate that inactivation of canonical Wnt signaling not only in ISCs/EBs and ECs, but also in EEs, can also impair ISC proliferation.

To further investigate the findings suggesting that inactivation of canonical Wnt signaling in EE cells could play a role in regulating ISC proliferation, we conducted experiments to assess the impact of *kmr* knockdown on both ISCs and EBs using Armadillo (Arm) as an indicator.

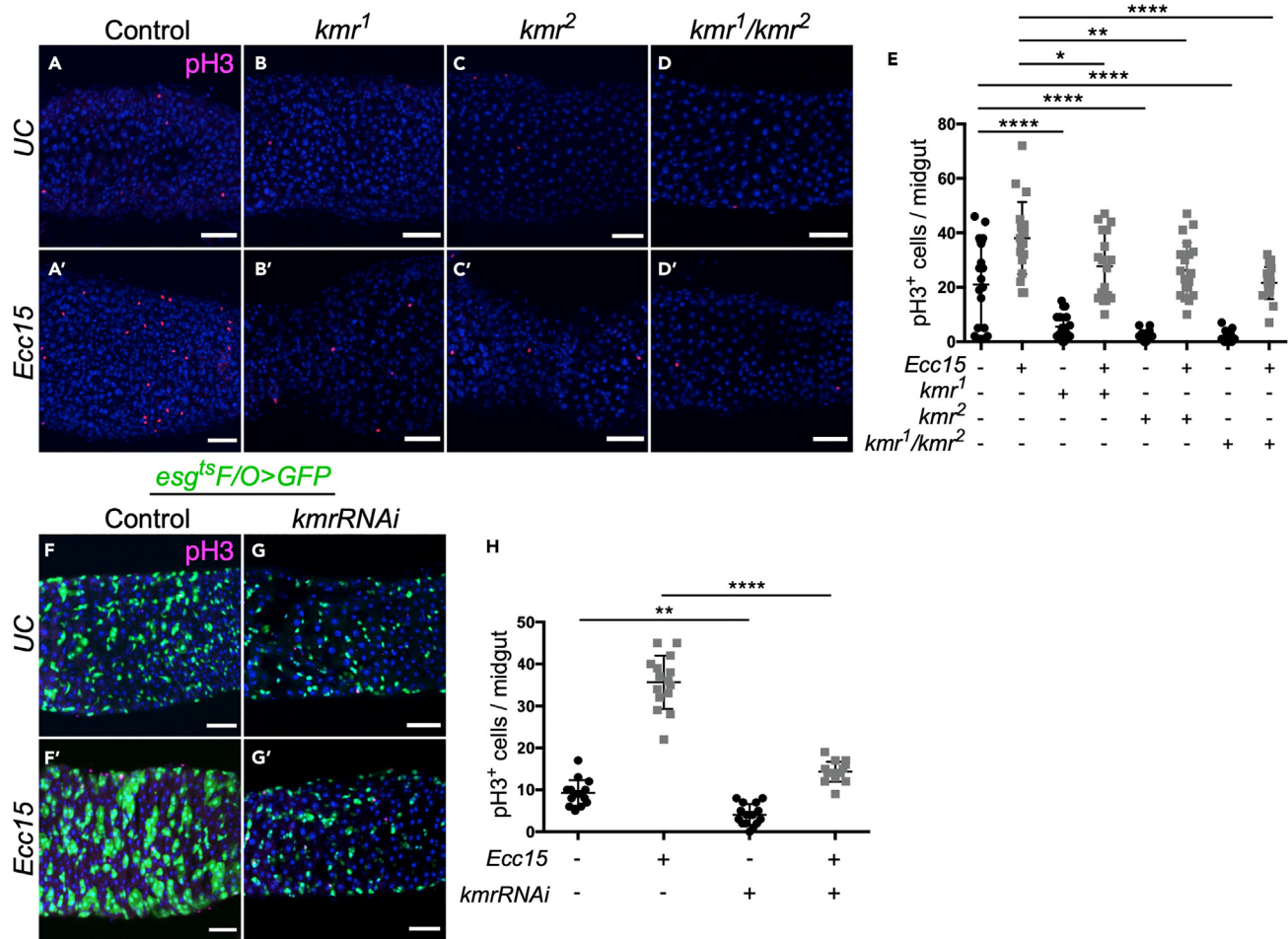


**Figure 2. Inactivation of *kramer* downregulates intestinal stem cell proliferation**

(A–E) *Kmr* knockout reduces intestinal stem cell proliferation in the midgut. Shown in (A–D) are representative confocal micrographs of number of phospho-histone H3-positive (pH3<sup>+</sup>) cells in the posterior midgut from unchallenged (UC) or *Ecc15*-challenged flies from the indicated genotypes: WT, *kmr* homozygous knockout (*kmr<sup>1</sup>* and *kmr<sup>2</sup>*), and compound heterozygote (*kmr<sup>1</sup>/kmr<sup>2</sup>*). Quantification of number of pH3<sup>+</sup> cells is shown in (E).

(F–H) Conditional *kmr* knockdown in ISCs and their progeny using the *esg<sup>ts</sup> F/O* system decreases number of pH3<sup>+</sup> cells in unchallenged and *Ecc15*-challenged conditions. Shown in (F and G) are representative confocal micrographs of posterior midgut. Magenta: pH3; green: GFP (RNAi); blue: DAPI. Quantification of number of pH3<sup>+</sup> cells from whole midguts are shown in (H) pH3<sup>+</sup> cells are quantified in the whole midgut of indicated genotype. One-way ANOVA with Tukey post-hoc: \*\*\*\*,  $p < 0.0001$ ; \*\*,  $p < 0.01$ ; \*,  $p < 0.05$ ; ns: not significant;  $n = 15–19$ . Scale bar: 40  $\mu\text{m}$ .

Double-staining of Arm and Prospero (Arm/Pro) enables identification of both progenitor cells (ISCs and EBs), which have high levels of membrane-associated Arm and lack of nuclear Pro staining, and pre-EE/EE cells, which exhibit strong nuclear Pro staining.<sup>39,40</sup> Intriguingly, *kmr* knockdown in ISCs/EBs (Figures 3J, 3K, and 3P) or in ECs (Figures 3L, 3M, and 3Q) caused no change in the number of Arm<sup>+</sup> ISC/EB cells, but *kmr* knockdown in EEs (Figures 3N, 3O, and 3R) resulted in significantly fewer ISC/EB cells compared to control, both in unchallenged and *Ecc15*-challenged flies. Consistent with these data, examination of number of ISC/EB cells using Arm/Pro staining following *kmr* knockdown using the *esg<sup>ts</sup> F/O* system revealed a decrease under both unchallenged and *Ecc15*-challenged conditions (Figure S6). Together, these results suggest that *kmr* knockdown, which inactivates canonical Wnt signaling in EEs, decreases ISC proliferation in a non-cell-autonomous manner.

### ***Kmr* is required for EE differentiation and maintenance**

The effects seen above of *kmr* and, by extension, Wnt signaling, in EEs came as a surprise, as there is a limited understanding of how Wnt signaling in this cell type might control ISC proliferation, prompting us to more deeply investigate this finding.<sup>11,28</sup> First, we hypothesized that *kmr*-dependent Wnt signaling in EEs might regulate the production and maintenance of EE cells themselves. To test this hypothesis, we examined Pro staining, as a marker of EEs, in WT and *kmr* knockout flies. We found that global *kmr* knockout decreased the number of Pro<sup>+</sup> (EE) cells in both unchallenged and *Ecc15*-challenged midguts (Figures 4A–4D).

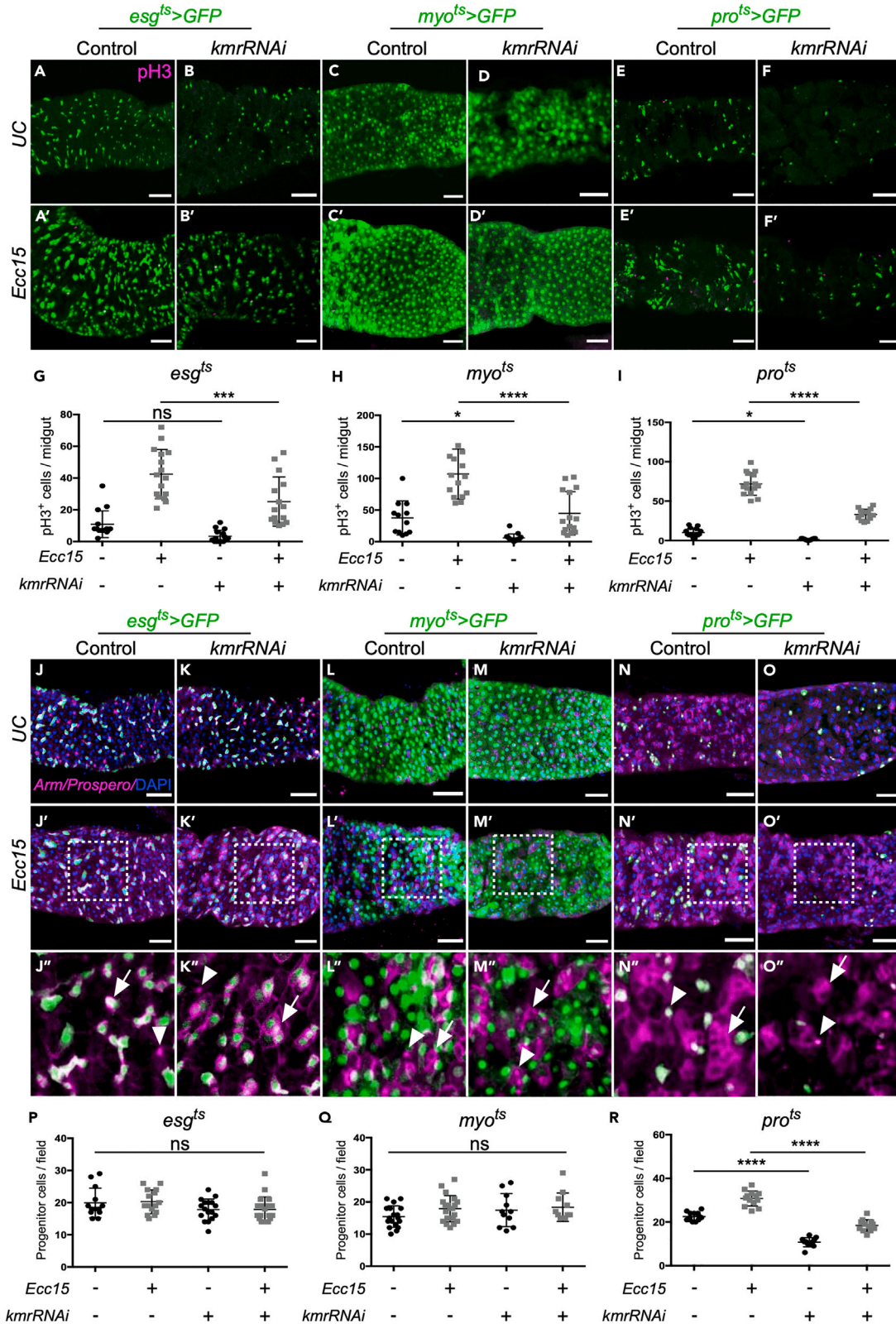


**Figure 3. Kramer knockdown in multiple cell types, including enteroendocrine cells, downregulates intestinal stem cell proliferation**

(A–I) RNAi-mediated knockdown of *kmr* in four different midgut cell types decreases number of pH3<sup>+</sup> proliferating cells under unchallenged (UC) and *Ecc15*-challenged conditions. *Kmr* RNAi is driven by the indicated promoter and marked by GFP expression: ISCs and EBs (*esg<sup>ts</sup>>GFP*), ECs (*myo<sup>ts</sup>>GFP*), and EEs (*pro<sup>ts</sup>>GFP*). Shown are representative confocal micrographs of posterior midguts. Green: GFP (RNAi); magenta: pH3<sup>+</sup> (proliferating cells). See also Figure S2 for monochrome images of pH3<sup>+</sup> fluorescence. Quantification of number of pH3<sup>+</sup> cells in the whole midgut of indicated genotype is shown in (G–I). (J–R) Knockdown of *kmr* only in EE cells, but not ISCs/EBs or ECs, causes a reduction of Armadillo<sup>+</sup>/Prospero<sup>-</sup> (Arm<sup>+</sup>/Pro<sup>-</sup>) ISCs. Midguts from unchallenged or *Ecc15*-challenged flies of the same genotypes as above were immunostained with antibodies against Armadillo, whose cortical localization indicates progenitor cells (example shown with arrow), and Prospero, whose nuclear localization indicates EEs (example shown with arrowhead). (J'–O') higher magnification of the boxed areas in (J'–O'). Quantification of number of progenitor (Arm<sup>+</sup>/Pro<sup>-</sup>) cells in same boxed areas in posterior midguts is shown in (P and Q). See Figure S6 for examination of number of progenitor cells in ISCs/EBs and their progeny using the *esg<sup>ts</sup> F/O* system. One-way ANOVA (Tukey post-hoc): \*\*\*\*\*,  $p < 0.0001$ ; \*\*\*,  $p < 0.001$ ; \*,  $p < 0.05$ ; ns: not significant;  $n = 11–18$ . Scale bars: 40  $\mu\text{m}$ .

Similar to previous experiments, we then disrupted *kmr* in different cell types in the midgut using RNAi-mediated knockdown. These studies revealed that *kmr* knockdown in ISCs/EBs (Figures 4E, 4F, and 4K), ECs (Figure 4G, 4H, and 4L), and EEs (Figures 4I, 4J, and 4M) all reduced the number of Pro<sup>+</sup> (EE) cells relative to control, in both unchallenged and *Ecc15*-challenged flies. We further used the *esg<sup>ts</sup> F/O* system to assess the extent of ISC differentiation into EEs and ECs 48 h post-induction of *kmr* knockdown. EEs were identified using Pro staining, and ECs were identified morphologically, based on their large nuclear and cytoplasmic size, within the GFP<sup>+</sup> population. We found that *kmr* knockdown reduced the number of Pro<sup>+</sup> cells and ECs under both unchallenged and *Ecc15*-challenged conditions (Figures 4N–4Q). These results suggest that *kmr* and, by extension, *kmr*-dependent Wnt signaling control the differentiation and maintenance of EEs in the midgut, though an alternate interpretation is that the pool of Pro<sup>+</sup> ISCs that give rise to pre-EEs are also affected by *kmr* knockdown.

**Regulation of the *kelch* E3 ubiquitin ligase adaptor by *kramer* controls proliferation in the midgut**

We next set out to examine the mechanism underlying the effects of *kmr* on ISC proliferation in the midgut. We have previously established the mammalian *kmr* ortholog PLEKHA4 as a positive regulator of DVL levels via sequestration and inactivation of the Cullin-3 substrate adaptor Kelch-like protein 12 (KLHL12) within clusters, preventing CUL3-KLHL12-mediated polyubiquitination of DVL, a key activator of Wnt/ $\beta$ -catenin and non-canonical Wnt signaling.<sup>22</sup> Therefore, we reasoned that the effects of *kmr* on ISC proliferation in the midgut might involve antagonism of a fly ortholog of KLHL12. We therefore investigated the genetic interaction of *kmr* with each of the two closest KLHL12 orthologs, *kelch* (*kel*), and *diablo* (*dbo*). We first assessed ISC proliferation by quantifying the number of pH3<sup>+</sup> cells in WT flies compared to those expressing cell type-specific *kel* RNAi in either ISCs/EBs (Figures S7A–S7E and S8A–S8D), ECs (Figures S7F–S7J and S8E–S8H), or EEs (Figures 5A–5E and S8I–S8L).

These studies revealed several findings. First, by comparing *kel* knockdown to control in *Ecc15*-challenged flies, it is apparent that *kel* knockdown in all cell types significantly increased total cell proliferation in the midgut, consistent for a role of *kel* as a suppressor of Wnt/ $\beta$ -catenin signaling via its polyubiquitination of Dsh (ISCs/EBs: Figure S7C and S7E; ECs: Figure S7H and S7J; EEs: Figures 5C and 5E).<sup>22</sup> The effect of *kel* RNAi in EE cells on this phenotype was strong enough to elicit a statistically significant increase in proliferating cells even in unchallenged flies (Figures 5C and 5E).

Second, we performed comparison of *kmr/kel* double knockdown flies to the three other groups (control and single knockdown of either *kmr* or *kel*). When such knockdown was performed in ISCs/EBs (Figures S7A–S7E) and in EEs (Figures 5A–5E), the *kmr/kel* double knockdown midguts exhibited an intermediate extent of proliferation: lower than *kel* knockdown, higher than *kmr* knockdown, and comparable to control. One interpretation of these results is that the addition of *kel* knockdown in the double knockdown strain significantly diminished the effects of single *kmr* knockdown on proliferation, consistent with a role for *kmr* as an inhibitor of *kel* as demonstrated biochemically for their mammalian orthologs, PLEKHA4 and KLHL12.<sup>22</sup> Furthermore, we found no effects of knockdown of *dbo*, the other potential KLHL12 fly ortholog, on this phenotype and no evidence for genetic interaction with *kmr* (Figure S9), further supporting a relationship between *kmr* and *kel* in controlling Wnt signaling in this tissue, consistent with our earlier studies.

However, the observed effects on proliferation were partial, i.e., proliferation in the double knockdown strain was not as high as *kel* knockdown alone. Though incomplete knockdown is a possible explanation for this intermediate result, the data are consistent with several types of genetic relationships between *kmr* and *kel*. Critically, they are identical to those that we observed in mammalian cells using RNAi-mediated knockdown of the orthologs of these genes, PLEKHA4 and KLHL12, alone or in combination.<sup>22</sup> Therefore, these results strongly suggest that the mechanism connecting *kmr* and *kel* in these cells is similar to that established by us and others as regulators of Wnt signaling pathways via effects on DVL/Dsh ubiquitination.<sup>22,41,42</sup> In ECs, we found that *kmr/kel* double knockdown nearly completely eliminated proliferation following *Ecc15* challenge, similar to *kmr* single knockdown, suggesting a different relationship between these genes in this cell type and one that may warrant further study (Figures S7F–S7J).

To measure the effects of *kmr* and/or *kel* knockdown on ISC/EB proliferation, we performed Arm/Pro staining on the double knockdown strains, as before (Figure 3). Our earlier results showed that *kmr* knockdown exclusively in EEs attenuated ISC proliferation (Figures 3N, 3O, and 3R). Here, we asked whether *kel* expression in EEs also regulates ISC proliferation, and whether *kel* knockdown could restore the reduction of ISC proliferation induced by *kmr* RNAi. As expected, given the lack of an effect of *kmr* knockdown in ISCs/EBs and ECs on this phenotype (Figure 3), individual knockdown of *kel* or combined *kmr/kel* double knockdown also had no effect on the number of Arm<sup>+</sup>/Pro<sup>-</sup> progenitors (Figure S10). By contrast, *kel* knockdown in EEs induced overproliferation of Arm<sup>+</sup>/Pro<sup>-</sup> progenitors (Figures 5F–5J) compared to control

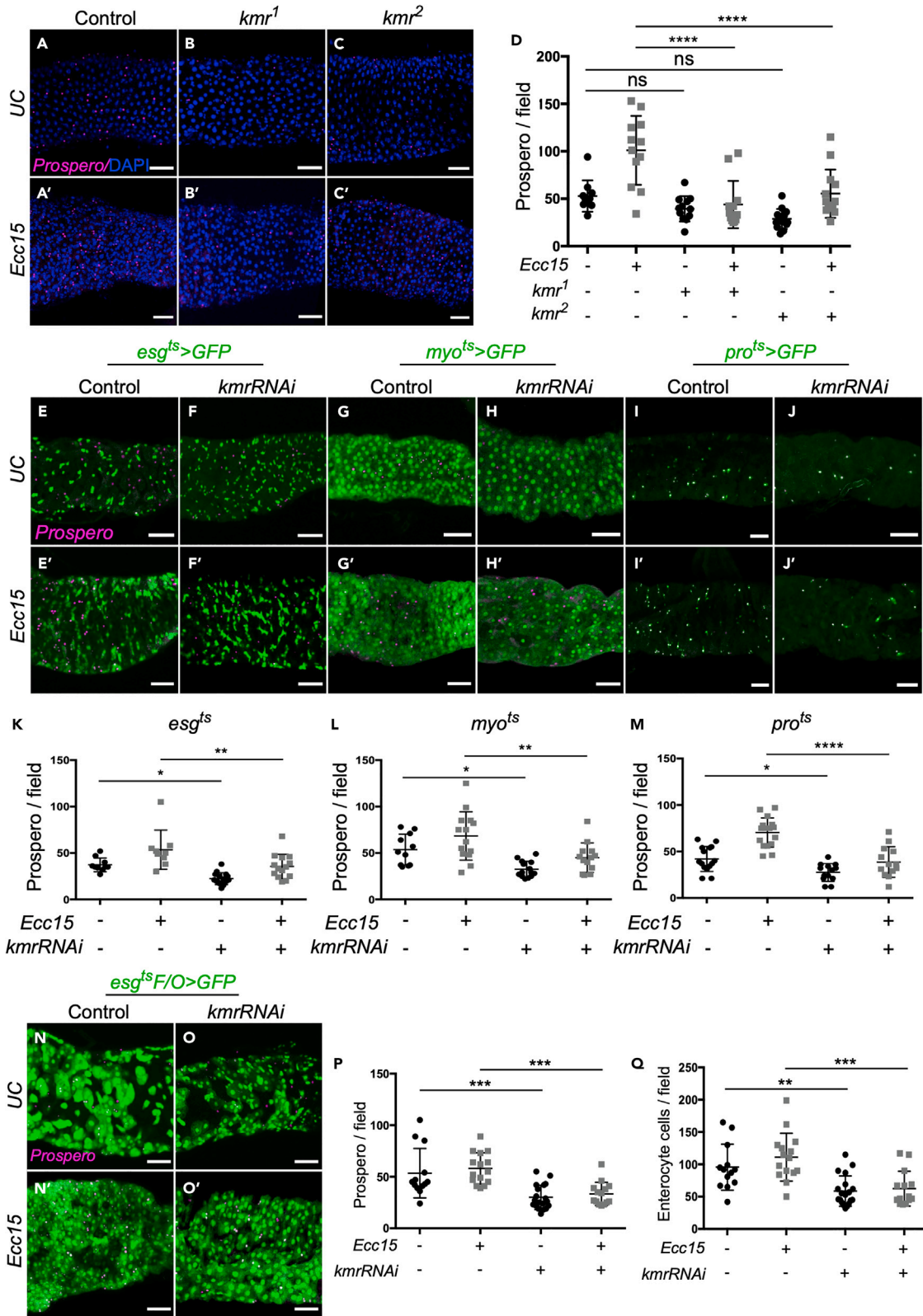


**Figure 4. Kramer knockdown impairs differentiation of enteroendocrine cells**

(A–D) *Kmr* knockout flies exhibit fewer EEs, marked with Prospero, compared to WT under unchallenged and *Ecc15*-challenged conditions, as shown by representative confocal micrographs in (A–C) (Magenta: anti-Prospero antibody; Blue: DAPI), with quantification of number of Pro<sup>+</sup> cells shown in (D). (E–M) Cell type-specific *kmr* knockdown in four cell types in the midgut causes decrease in the number of EEs in the midgut relative to control under unchallenged and *Ecc15*-challenged conditions, as shown by representative confocal micrographs in (E–J) (Magenta: anti-Prospero antibody; Green: GFP (RNAi)), with quantification of number of Pro<sup>+</sup> cells shown in (K–M). (N–Q) Conditional *kmr* knockdown in ISCs and their progeny using the *esg<sup>ts</sup> F/O* system decreases number of Pro<sup>+</sup> and enterocyte (EC) cells 48 h post-induction of *esg<sup>ts</sup> F/O* under both unchallenged (UC) and *Ecc15*-challenged conditions. Representative images of posterior midguts are shown in N and quantification of number of Pro<sup>+</sup> and ECs shown in (P and Q). Pro<sup>+</sup> (magenta) and ECs (green, identified by morphology) were quantified from the same fields of view. One-way ANOVA (Tukey post-hoc): \*\*\*\*,  $p < 0.0001$ ; \*\*,  $p < 0.01$ ; \*,  $p < 0.05$ ; ns: not significant;  $n = 9–15$ . Scale bars: 40  $\mu\text{m}$ .

and fully eliminated the effect of *kmr* knockdown in reducing ISC proliferation. Taken together, these results indicate that *kmr* and *kelch* regulate ISC proliferation in the midgut in a manner consistent to previous mechanistic findings in mammalian cells and other tissues in adult and larval *Drosophila*, where PLEKHA4/*kmr* was found to enhance both canonical Wnt/ $\beta$ -catenin and PCP, a non-canonical Wnt signaling pathway.<sup>22</sup>

To investigate the relationship between *kmr* and *kel*, we first examined *kel* mRNA levels and found that *kmr* knockdown led to a trend toward reduction in *kel* expression upon *Ecc15* challenge (Figure 5K), consistent with findings that knockdown of the mammalian *kmr* ortholog, PLEKHA4, reduced levels of the *kel* ortholog KLHL12.<sup>22</sup> To more directly assess the role of the Kelch protein on Dsh in this system, i.e., interactions with Dsh and role in Dsh polyubiquitination, we performed heterologous expression and co-immunoprecipitation (coIP) of tagged versions of the relevant *Drosophila* proteins in a human cell line. In these studies, we co-expressed *Drosophila* FLAG-Dsh, mScarlet-i-Kelch (mSc-i-Kel), and HA-ubiquitin (HA-Ub) in HEK 293T cells and performed anti-FLAG IP. We found that FLAG-Dsh indeed interacted with mSc-i-Kel and that forced overexpression of mSc-i-Kel induced a significant increase in the extent of polyubiquitination of Dsh compared controls (Figures 5L, 5M, and S11). These findings align with those of the mammalian orthologs of these proteins, KLHL12 and DVL,<sup>22,41</sup> supporting a conserved role in *Drosophila* for Kel as a positive regulator of Dsh polyubiquitination and *Kmr* as a negative regulator of Kel action in this pathway.

***Kmr* controls ISC proliferation via effects on both canonical and non-canonical Wnt signaling**

Because PLEKHA4/*kmr* regulates DVL/Dsh levels, which can affect both canonical and non-canonical Wnt signaling pathways, a key outstanding question is whether the effects of *kmr* observed here on ISC proliferation in the midgut are due entirely to Wnt/ $\beta$ -catenin signaling, PCP or another non-canonical pathway, or a combination. Resolving this distinction is important because, though previous work from our lab established PLEKHA4 as a regulator of Wnt/ $\beta$ -catenin signaling in mammalian cells, in *Drosophila*, we found it to regulate hair polarization, a hallmark PCP phenotype, in several tissues, consistent with previous studies implicating *kel* and *dbo* in PCP signaling.<sup>42</sup> To date, no studies have found that *kmr* controls Wnt/ $\beta$ -catenin signaling.

*Kmr* knockdown globally and in relevant midgut cell types individually all caused a decrease in expression of the *fz3-RFP* reporter of canonical Wnt signaling, indicating that *kmr* is indeed capable of regulating this pathway in the midgut (Figure 1). However, whether the observed effects of *kmr* on ISC proliferation elsewhere in this study (Figures 2, 3, 4, and 5) are due to effects on canonical Wnt signaling and/or PCP remain undetermined. To distinguish between these possibilities, we inactivated each of those pathways individually in ISCs/EBs, ECs, or EEs, to determine which perturbation would phenocopy *kmr* knockdown. To target PCP, we used knockdown of *otk*, the *Drosophila* ortholog of PTK7, a cell-surface receptor that regulates PCP,<sup>28</sup> and to inactivate canonical Wnt/ $\beta$ -catenin, we performed knockdown of *pangolin* (*pan*), the *Drosophila* TCF/LEF ortholog that acts as a transcription factor downstream of Arm ( $\beta$ -catenin).<sup>29</sup>

We first evaluated overall proliferation in the midgut using pH3 staining (Figures 6A–6L and S12). We found that in *Ecc15*-challenged flies, *otk* knockdown in ISCs/EBs (Figures 6A, 6B, and 6D) and in EEs (Figures 6I, 6J, and 6L) but not in ECs (Figures 6E, 6F, and 6H) reduced overall proliferation. By contrast, *pan* knockdown in all cell types significantly reduced proliferation (ISCs/EBs: Figures 6A, 6C, and 6D; ECs; Figures 6E, 6G, and 6H; EEs; Figures 6I, 6K, and 6L). These results indicate that *pan* knockdown exactly phenocopies *kmr* knockdown in regulation of stem cell proliferation, suggesting that *kmr* acts on these phenotypes through canonical Wnt signaling. At the same time, these data indicate important roles for Wnt/ $\beta$ -catenin signaling not only within ISCs/EBs and ECs, as was previously known, but also in EEs, in controlling proliferation. The effects of *otk* knockdown on proliferation partially phenocopies *kmr* knockdown, suggesting that *kmr* regulation of PCP may be relevant within progenitors, consistent with its role in regulation of PCP in other tissues.<sup>22</sup> The *otk* knockdown experiments confirm recent studies showing a role for PCP within ISCs for controlling proliferation,<sup>28</sup> and they also reveal unknown potential roles for PCP within Pro<sup>+</sup> cells in regulating proliferation.

Finally, we used Arm/Pro staining to quantify effects of *otk* or *pan* knockdown in EEs on ISC/EB proliferation (Figures 6M–6P), given the strong effects of *kmr* knockdown in these cells on this phenotype (Figures 3N, 3O, and 3R). We found that *otk* knockdown in EE cells had no effect on the number of Arm<sup>+</sup>/Pro<sup>+</sup> cells both in unchallenged conditions and following *Ecc15* challenge (Figures 6M, 6N, and 6P). By contrast, *pan* knockdown impaired stem cell proliferation by this readout compared to control, both in unchallenged and *Ecc15*-challenged flies (Figures 6M, 6O, and 6P). These results indicate that *kmr* within Pro<sup>+</sup> cells regulates stem cell proliferation in the midgut via canonical Wnt signaling. More broadly, our results implicate *kmr* as a new regulator of canonical Wnt signaling in the fly midgut via effects on several pathways, and our data suggest unexpected roles for Wnt signaling within EEs in the regulation of stem cell proliferation in the construction of the gut epithelium in *Drosophila* (Figure 7).

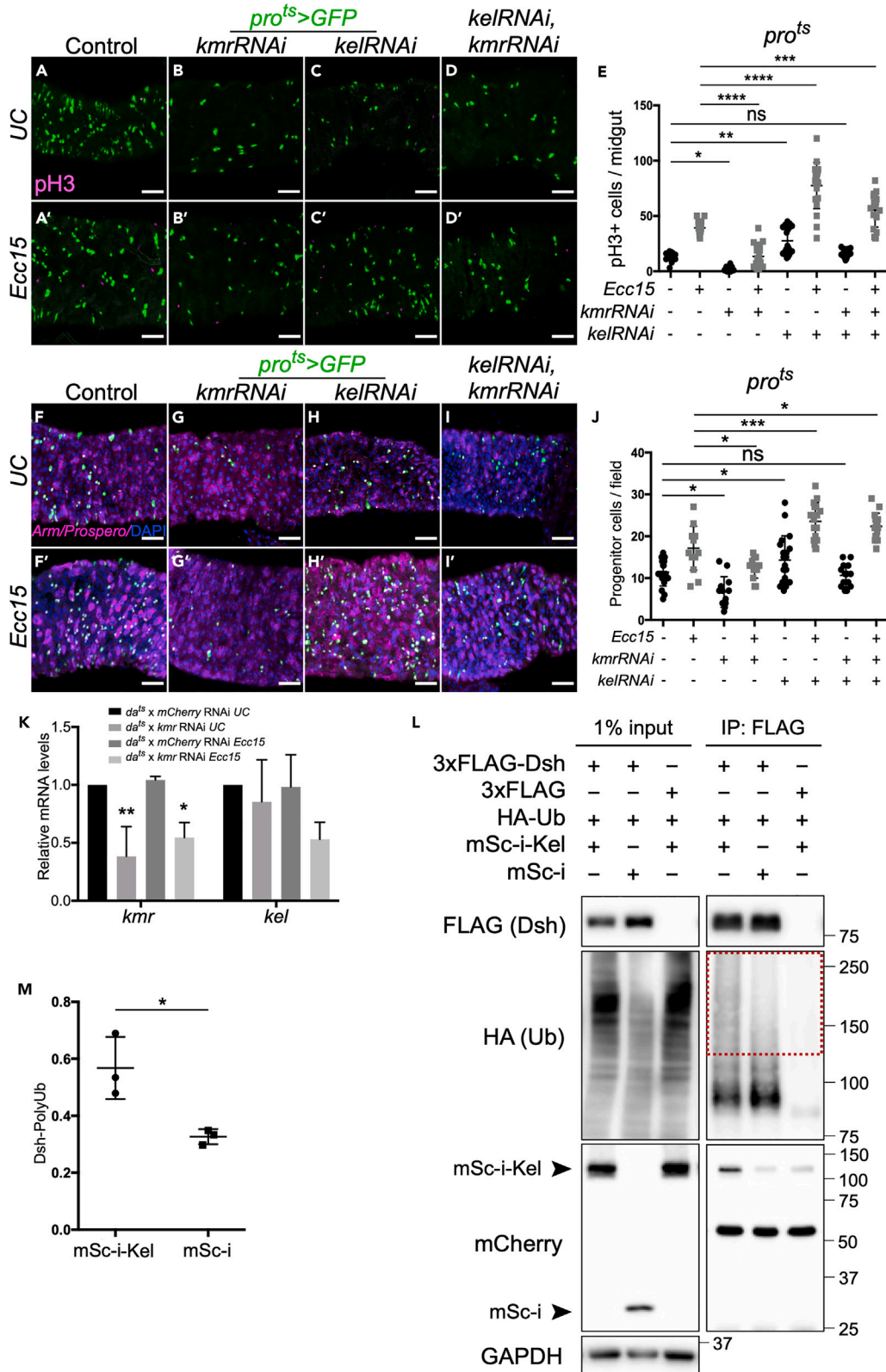


**Figure 5. Knockdown of *kelch* partially reverses the defects in intestinal stem cell proliferation caused by *kramer* downregulation in midgut cells, achieved through the attenuation of Dsh ubiquitination by downregulation of *kelch***

(A–E) Examination of number of pH3<sup>+</sup> cells in the midgut in unchallenged or *Ecc15*-challenged flies expressing conditional, cell type-specific knockdown of *kmr* and/or the Cullin-3 E3 ligase substrate-specific adaptor *kelch* (*kel*) in EEs (*pro<sup>ts</sup>>GFP*). Shown for each set are representative confocal micrographs (magenta: pH3; green: GFP [RNAi]) and quantification of number of pH3<sup>+</sup> cells in the whole midgut. See also Figure S8 for monochrome images of pH3 staining and Figure S9 for examination of effects of the *kel* paralog *diablo* (*dbo*).

(F–J) Examination of number of Arm<sup>+</sup>/Pro<sup>−</sup> progenitor cells in the midgut in unchallenged or *Ecc15*-challenged flies expressing conditional, cell type-specific knockdown of *kmr* and/or *kel* in EEs. Shown are representative confocal micrographs (magenta: Arm/Pro; green: GFP [RNAi]) and quantification of number of Arm<sup>+</sup>/Pro<sup>−</sup> cells in the same field of posterior midguts. See Figure S10 for similar analysis of Arm<sup>+</sup>/Pro<sup>−</sup> cells in ISC/EB or EC-specific knockdown of *kmr* and/or *kel*. *n* = 12–18. Scale bars: 40 μm.

(K) RT-qPCR analysis of *kmr* and *kel* levels in the midgut upon global *kmr* knockdown and *mCherry* RNAi was used as a negative control. Values represent fold change in mRNA levels, normalized to the unchallenged control (*n* = 3).

(L) Assessment of extent of interaction of 3xFLAG-Dsh and mScarlet-i-Kelch (mSc-i-Kel) by co-immunoprecipitation (IP) and extent of 3xFLAG-Dsh ubiquitination induced by forced expression of mSc-i-Kel, relative to controls (e.g., 3xFLAG or mSc-i empty vectors as indicated). HEK 293T cells were transfected with indicated constructs encoding tagged *Drosophila* proteins, and lysates were generated, subjected to cells post-transfection were processed for anti-FLAG IP, and analyzed by western blot.

(M) Quantification of polyubiquitination of 3xFLAG-Dsh under forced overexpression of mSc-i-Kel compared to mSc-i only. The plot indicates quantification of the region boxed in red in (L) *n* = 3. One-way ANOVA (Tukey post-hoc): \*\*\*\*, *p* < 0.0001; \*\*\*, *p* < 0.001; \*\*, *p* < 0.01; \*, *p* < 0.05; ns, not significant.

## DISCUSSION

Proliferation and differentiation of ISCs in the adult *Drosophila* midgut are essential to maintain the balance of tissue homeostasis and prevent excessive proliferation in this tissue. Wnt/β-catenin signaling plays central roles in tissue maintenance during development, including in the midgut. However, how canonical Wnt signaling is activated within ISC progenitors and by fully differentiated progeny cells is still not well understood. Here, we discovered a new player, *kramer* (*kmr*), that regulates canonical Wnt signaling in the *Drosophila* midgut using a challenge with the non-lethal pathogen *Erwinia carotovora carotovora 15* (*Ecc15*) to induce massive ISC proliferation required to rebuild the damaged gut epithelium.

Using this system, we established *kmr* as a positive regulator of ISC proliferation and Wnt/β-catenin signaling. We then used inducible, cell type-specific *kmr* knockdown as a tool to interrogate the requirements for Wnt signaling within each cell type in the gut for controlling ISC proliferation. In addition to known effects of Wnt signaling within ISCs, their immediate downstream progenitors termed EBs, and fully differentiated ECs in governing this process, our study points to unexpected roles for Wnt signaling within EEs as a mechanism controlling stem cell proliferation in the *Drosophila* midgut.

We first showed that interruption of *kmr* function decreases the expression of a canonical Wnt signaling target gene, *fz3*, in the posterior midgut, consistent with studies demonstrating *fz3-RFP* expression in both ISCs and ECs and showing that knockout of Wnt signaling components led to loss of *fz3* expression in the posterior-most portion of region R5 of the midgut.<sup>36</sup> Though ECs are the major cell type in which Wnt signaling is activated,<sup>26,36,39</sup> our studies using *kmr* knockdown in multiple cell types suggest that Wnt signaling is also active in ISCs/EBs and EEs in posterior end of the midgut. These studies also revealed that loss of *kmr* in multiple cell types results in fewer EE cells and decreased ISC proliferation in the posterior midgut, indicating a role for *kmr* in EE differentiation.

Further, *kmr* knockdown in all cell types caused a decrease in proliferating, phospho-H3 positive (pH3<sup>+</sup>) cells, though staining with Armadillo/Prospero antibodies, which enables identification of ISCs/EBs and EEs, suggests that *kmr* knockdown in EE cells specifically down-regulates stem cell proliferation. This distinction is important because pH3<sup>+</sup> cells include all dividing progenitor cells, including ISCs/EBs and pre-EEs, and our data showed that *kmr* knockdown in all cell types significantly decreased dividing stem cells. The mechanisms underlying how *kmr* knockdown within EEs affects ISC proliferation remain unknown and will be the focus of future studies, possibly involving analysis of isolated EEs.

Notably, *kmr* knockdown in ISCs/EBs and in ECs did not result in a defect in the number of Arm<sup>+</sup>/Pro<sup>−</sup> cells (i.e., ISCs/EBs). However, *kmr* knockdown in Pro<sup>+</sup> cells led to a reduction in the number of ISCs/EBs, suggesting that *kmr* expression in EE cells regulates the proliferation of neighboring ISCs in a non-autonomous manner. These data also provide support to a model wherein EEs derive not from EBs<sup>11,12</sup> but instead from a distinct set of progenitors termed pre-EEs.<sup>7,30,31</sup>

Intriguingly, our findings appear to contrast with previous research demonstrating the non-autonomous prevention of excess ISC proliferation by inhibition of JAK/STAT signaling upon the activation of Wnt signaling in ECs.<sup>39</sup> There are several potential reasons for these differing results. First, our study focuses on the posterior-most portion of the R5 region of the midgut, which is characterized by high levels of Wnt pathway activation, whereas the previous work examined a broader portion of the posterior midgut, encompassing the entire R4 and R5 regions. Crucially, a key finding of the previous study was that the ADP-ribose polymerase Tankyrase, typically regarded as a Wnt activator, is critical for signaling in regions with relatively low Wnt pathway activation but not required for Wnt target gene activation in regions with high pathway activation. Second, we observed that, though expression of the JAK/STAT ligands *upd2* and *upd3* increased upon *Ecc15* infection as expected, *kmr* knockdown in ECs or in EEs had no effect or very modest effect on *upd2* and *upd3* levels (Figure S13).<sup>39</sup> Because these results rely on RT-qPCR analysis of mRNA levels in whole tissues, however, they are unable to establish the epistatic relationship between *kmr* and JAK/STAT signaling. Taken together, we conclude that the role of *kmr* in these pathways in this tissue, and their effects on ISC proliferation, is more complex and will require further studies to elucidate how *kmr* expression within EEs non-autonomously regulates proliferation of neighboring ISCs.

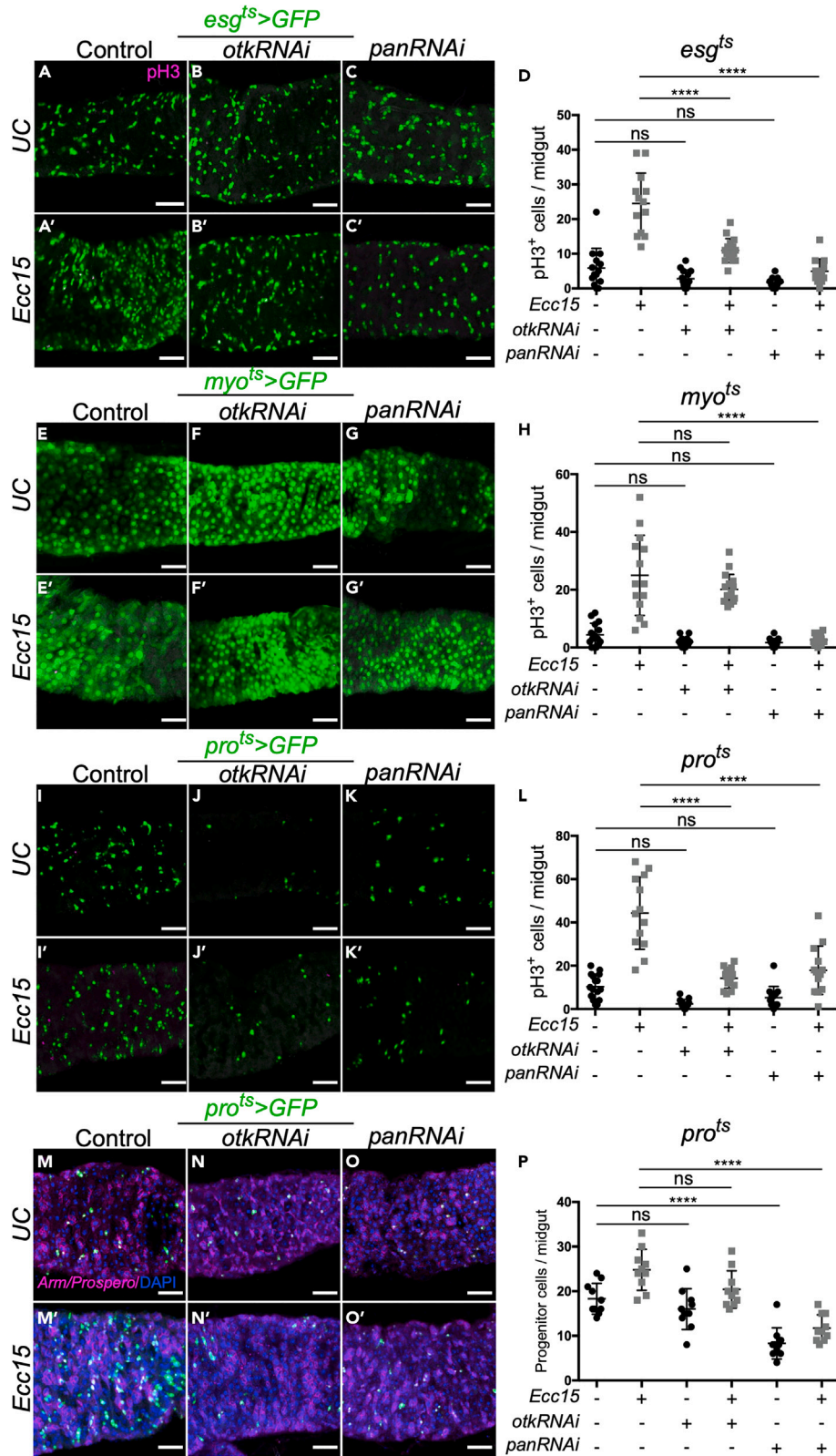


**Figure 6. Suppression of Wnt/ $\beta$ -catenin signaling using *pangolin* (*pan*) knockdown, but not of planar cell polarity using *off-track* (*otk*) knockdown, phenocopies effects of *kmr* knockdown on intestinal stem cell proliferation in the midgut**

(A–L) Examination of number of pH3<sup>+</sup> cells in the midgut in unchallenged or *Ecc15*-challenged flies expressing conditional, cell type-specific knockdown of *pan* or *otk* in ISCs/EBs (A–D, *esg<sup>ts</sup>>GFP*), ECs (E–H, *myo<sup>ts</sup>>GFP*), or EEs (I–L, *pro<sup>ts</sup>>GFP*). Shown for each set are representative confocal micrographs (magenta: pH3; green: GFP [RNAi]) and quantification of number of pH3<sup>+</sup> cells. See also Figure S12 for monochrome images of pH3 staining.

(M–P) Examination of number of Arm<sup>+</sup>/Pro<sup>-</sup> progenitor cells in the midgut in unchallenged or *Ecc15*-challenged flies expressing conditional, cell type-specific knockdown of *pan* or *otk* in EEs. Shown are representative confocal micrographs (magenta: Arm/Pro; green: GFP [RNAi]) and quantification of number of Arm<sup>+</sup>/Pro<sup>-</sup> cells. One-way ANOVA (Tukey post-hoc): \*\*\*\*,  $p < 0.0001$ ; ns, not significant;  $n = 11–14$ . Scale bars: 40  $\mu$ m.

Our study also sheds light on the mechanisms by which *kmr* expression in distinct midgut cell types might regulate the physiological response to *Ecc15* infection. Prior work on the mammalian ortholog of *kmr*, PLEKHA4, revealed that it promotes Wnt signaling pathways via physical interaction with KLHL12, a CUL3 E3 ubiquitin ligase substrate-specific adaptor and negative regulator of DVL.<sup>22</sup> By binding to KLHL12 and sequestering it in plasma membrane-associated clusters, PLEKHA4 prevents DVL polyubiquitination by CUL3-KLHL12, ultimately causing elevated DVL levels and enhanced Wnt signaling in Wnt-receiving cells.

Because of the pleiotropic roles for DVL in both canonical Wnt/ $\beta$ -catenin and non-canonical  $\beta$ -catenin-independent pathways,<sup>20</sup> we found that PLEKHA4 knockdown affected both of these pathways.<sup>22</sup> Our previous studies on *kmr* in *Drosophila*, focusing on hair patterning, identified defects in PCP, a Frizzled- and Dsh-dependent pathway in flies.<sup>22</sup> However, the present study identifies for the first time a role for *kmr* in promoting canonical Wnt/ $\beta$ -catenin signaling *in vivo*. By analyzing knockdown of the two fly KLHL12 orthologs, *kelch* and *diablo*, we found that *kmr* acts in opposition to *kelch*, much as PLEKHA4 does with KLHL12 in mammalian cells, supporting the established mechanism of action. Finally, we independently blocked Wnt/ $\beta$ -catenin and PCP signaling and assessed ISC proliferation following *Ecc15* challenge and found that only blockade of Wnt/ $\beta$ -catenin signaling exactly phenocopied loss of *kmr*.

In conclusion, our study reveals that the Dsh regulator *kmr* is a new, important regulator of Wnt/ $\beta$ -catenin signaling and ISC proliferation *in vivo*. As well, we harness *kmr* as a tool to systematically investigate the role of Wnt signaling in each of the major cell types in the *Drosophila* midgut in controlling ISC proliferation and differentiation during epithelial repair following challenge with an enteric pathogen. These studies suggest that Wnt signaling within EEs can control this process, adding a new layer of regulation to this important physiological process. Future studies will be necessary to identify downstream mechanisms by which EEs may non-autonomously regulate ISC proliferation in the midgut, as well as the existence of similar pathways in mammalian systems.

**Limitations of the study**

This study elucidates that *kramer* (*kmr*) expression in multiple intestinal cell types promotes ISC proliferation by modulation of Wnt/ $\beta$ -catenin signaling. However, the molecular mechanisms by which *kmr*-dependent Wnt signaling in non-ISC cells non-autonomously affects ISC

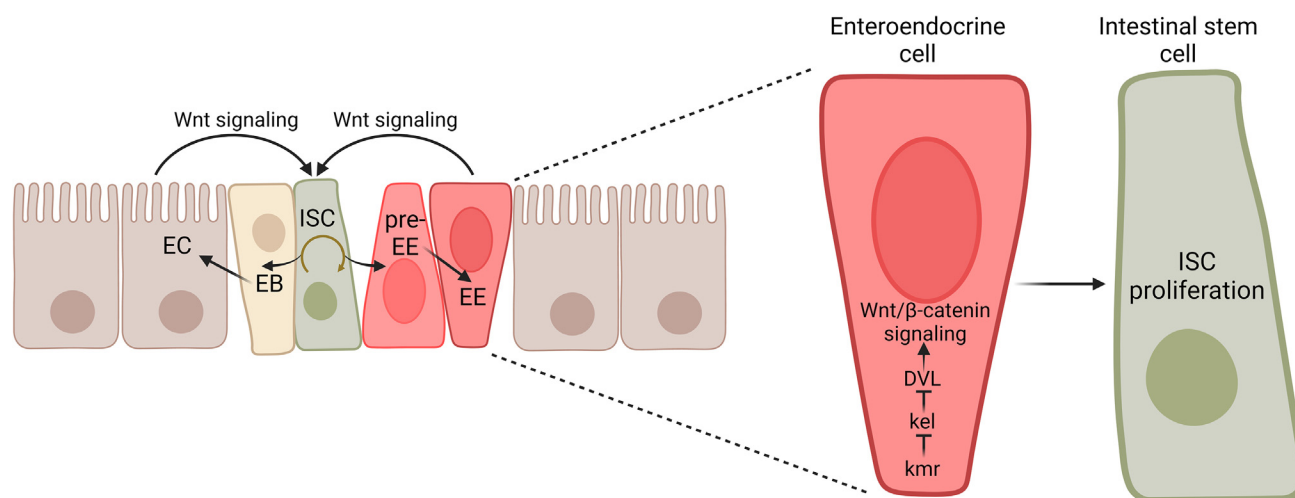


**Figure 7. Working model for *kramer* function in the *Drosophila* midgut**

Intestinal epithelial homeostasis requires continuous ISC self-renewal and differentiation into other cell types, including enteroblasts (EB) that give rise to enterocytes (EC), and enteroendocrine cells (EEs) that derive from a distinct progenitor termed pre-EEs. In turn, these multiple cell types can provide signaling including secreted Wnt ligands to sustain ISC proliferation. In this model, canonical Wnt/ $\beta$ -catenin signaling within multiple cell types, including enteroendocrine cells, promotes stem cell proliferation in the midgut. Such signaling is dependent upon *kramer*, which acts by antagonizing *kelch*, a negative regulator of DVL/Dsh and Wnt signaling pathways.

proliferation remain unknown. In particular, our data support a role for Wnt signaling within EE cells in regulating ISC proliferation, but technical challenges prevented us from being able to carry out a detailed investigation of changes occurring within *kmr*-deficient EEs. For example, the effects of *kmr* loss were investigated at the whole-tissue level by RT-qPCR and at the single-cell level by immunofluorescence, and examination of effects on a wider set of targets under various perturbations would require either EE isolation or generation of additional antibodies to relevant targets. Notably, the lack of an antibody capable of detecting endogenous Kmr prevented us from definitively establishing the levels and subcellular localization of the Kmr protein in the basal state and upon *Ecc15* challenge. Finally, though heterologous expression of *Drosophila* Kel and Dsh within HEK 293T cells supports an evolutionarily conserved interaction between these proteins consistent with previous studies on KLHL12 and DVL2/3, the biochemical interactions of Kmr with *Drosophila* Kel and Dsh were not explored. The large size of the predicted open reading frame of Kmr, which includes lengthy low complexity, repetitive sequences that are not present in its mammalian homologs, may complicate efforts to elucidate the relevant biomolecular interactions involved in this pathway.

## STAR★METHODS

Detailed methods are provided in the online version of this paper and include the following:

- KEY RESOURCES TABLE
- RESOURCE AVAILABILITY
  - Lead contact
  - Materials availability
  - Data and code availability
- EXPERIMENTAL MODEL AND STUDY PARTICIPANT DETAILS
  - Fly stock generation and husbandry
  - Mammalian cell culture
- METHOD DETAILS
  - Infection of flies with *Ecc15*
  - Immunohistochemistry and histology
  - qRT-PCR
  - Plasmids and cloning
  - Transfection of HEK 293T cells
  - Cell lysis and preparation of whole cell lysates for SDS-PAGE
  - Immunoprecipitation
  - SDS-PAGE and Western blotting
- QUANTIFICATION AND STATISTICAL ANALYSIS
  - Statistical analysis

## SUPPLEMENTAL INFORMATION

Supplemental information can be found online at <https://doi.org/10.1016/j.isci.2024.110113>.

## ACKNOWLEDGMENTS

We acknowledge support from the NIH (J.M.B.: R01GM131101; N.B.: R01AI148529, R21AG065733, and R01AI148541), the NSF (N.B.: IOS1656118), and the Sloan Foundation (J.M.B.: Sloan Research Fellowship). We thank Yashi Ahmed (Dartmouth) for providing *fz3-RFP* flies, Lin Luan for technical assistance, the Han lab for equipment, and Chun Han and members of the Baskin lab for helpful discussions. Graphical abstract and Figure 7 were created with [Biorender.com](https://biorender.com).

## AUTHOR CONTRIBUTIONS

Conceptualization: H.S., A.S., D.C., A.B., N.B., and J.M.B.; funding Acquisition: J.M.B. and N.B.; investigation: H.S., A.S., D.C., and A.B.; project administration: J.M.B.; supervision: J.M.B.; writing – original draft: H.S. and J.M.B.; writing – review and editing: H.S., A.S., D.C., A.B., N.B., and J.M.B.

## DECLARATION OF INTERESTS

The authors declare no competing interests.

Received: February 23, 2023

Revised: March 8, 2024

Accepted: May 23, 2024

Published: May 27, 2024

## REFERENCES

- Buchon, N., Broderick, N.A., Poidevin, M., Pradervand, S., and Lemaitre, B. (2009). *Drosophila* intestinal response to bacterial infection: activation of host defense and stem cell proliferation. *Cell Host Microbe* 5, 200–211. <https://doi.org/10.1016/j.chom.2009.01.003>.
- Chen, K., Luan, X., Liu, Q., Wang, J., Chang, X., Snijders, A.M., Mao, J.-H., Secombe, J., Dan, Z., Chen, J.-H., et al. (2019). *Drosophila* Histone Demethylase KDM5 Regulates Social Behavior through Immune Control and Gut Microbiota Maintenance. *Cell Host Microbe* 25, 537–552.e8. <https://doi.org/10.1016/j.chom.2019.02.003>.
- O'Brien, L.E., Soliman, S.S., Li, X., and Bilder, D. (2011). Altered modes of stem cell division drive adaptive intestinal growth. *Cell* 147, 603–614. <https://doi.org/10.1016/j.cell.2011.08.048>.
- Buchon, N., Broderick, N.A., Kuraishi, T., and Lemaitre, B. (2010). *Drosophila* EGFR pathway coordinates stem cell proliferation and gut remodeling following infection. *BMC Biol.* 8, 152. <https://doi.org/10.1186/1741-7007-8-152>.
- Bonfini, A., Dobson, A.J., Duneau, D., Revah, J., Liu, X., Houtz, P., and Buchon, N. (2021). Multiscale analysis reveals that diet-dependent midgut plasticity emerges from alterations in both stem cell niche coupling and enterocyte size. *Elife* 10, e64125. <https://doi.org/10.7554/eLife.64125>.
- Miguel-Aliaga, I., Jasper, H., and Lemaitre, B. (2018). Anatomy and Physiology of the Digestive Tract of *Drosophila melanogaster*. *Genetics* 210, 357–396. <https://doi.org/10.1534/genetics.118.300224>.
- Zeng, X., and Hou, S.X. (2015). Enteroendocrine cells are generated from stem cells through a distinct progenitor in the adult *Drosophila* posterior midgut. *Development* 142, 644–653. <https://doi.org/10.1242/dev.113357>.
- Radtke, F., and Clevers, H. (2005). Self-Renewal and Cancer of the Gut: Two Sides of a Coin. *Science* 307, 1904–1909. <https://doi.org/10.1126/science.1104815>.
- Morrison, S.J., and Spradling, A.C. (2008). Stem cells and niches: mechanisms that promote stem cell maintenance throughout life. *Cell* 132, 598–611. <https://doi.org/10.1016/j.cell.2008.01.038>.
- Amcheslavsky, A., Song, W., Li, Q., Nie, Y., Bragatto, I., Ferrandon, D., Perrimon, N., and Ip, Y.T. (2014). Enteroendocrine Cells Support Intestinal Stem-Cell-Mediated Homeostasis in *Drosophila*. *Cell Rep.* 9, 32–39. <https://doi.org/10.1016/j.celrep.2014.08.052>.
- Beehler-Evans, R., and Micchelli, C.A. (2015). Generation of enteroendocrine cell diversity in midgut stem cell lineages. *Development* 142, 654–664. <https://doi.org/10.1242/dev.114959>.
- Dutta, D., Dobson, A.J., Houtz, P.L., Gläßer, C., Revah, J., Korzelius, J., Patel, P.H., Edgar, B.A., and Buchon, N. (2015). Regional Cell-Specific Transcriptome Mapping Reveals Regulatory Complexity in the Adult *Drosophila* Midgut. *Cell Rep.* 12, 346–358. <https://doi.org/10.1016/j.celrep.2015.06.009>.
- Tian, A., Benchabane, H., and Ahmed, Y. (2018). Wingless/Wnt Signaling in Intestinal Development, Homeostasis, Regeneration and Tumorigenesis: A *Drosophila* Perspective. *J. Dev. Biol.* 6, E8. <https://doi.org/10.3390/jdb6020008>.
- Fevr, T., Robine, S., Louvard, D., and Huelsken, J. (2007). Wnt/beta-catenin is essential for intestinal homeostasis and maintenance of intestinal stem cells. *Mol. Cell Biol.* 27, 7551–7559. <https://doi.org/10.1128/MCB.01034-07>.
- Mah, A.T., Yan, K.S., and Kuo, C.J. (2016). Wnt pathway regulation of intestinal stem cells. *J. Physiol.* 594, 4837–4847. <https://doi.org/10.1113/JP271754>.
- Wikramanayake, A.H., Hong, M., Lee, P.N., Pang, K., Byrum, C.A., Bince, J.M., Xu, R., and Martindale, M.Q. (2003). An ancient role for nuclear  $\beta$ -catenin in the evolution of axial polarity and germ layer segregation. *Nature* 426, 446–450. <https://doi.org/10.1038/nature02113>.
- Cancer Genome Atlas Network (2012). Comprehensive molecular portraits of human breast tumors. *Nature* 490, 61–70. <https://doi.org/10.1038/nature11412>.
- Rim, E.Y., Clevers, H., and Nusse, R. (2022). The Wnt Pathway: From Signaling Mechanisms to Synthetic Modulators. *Annu. Rev. Biochem.* 91, 571–598. <https://doi.org/10.1146/annurev-biochem-040320-103615>.
- Albrecht, L.V., Tejada-Muñoz, N., and De Robertis, E.M. (2021). Cell Biology of Canonical Wnt Signaling. *Annu. Rev. Cell Dev. Biol.* 37, 369–389. <https://doi.org/10.1146/annurev-cellbio-120319-023657>.
- Wallingford, J.B., and Habas, R. (2005). The developmental biology of Dishevelled: an enigmatic protein governing cell fate and cell polarity. *Development* 132, 4421–4436. <https://doi.org/10.1242/dev.02068>.
- Miyazaki, K., Fujita, T., Ozaki, T., Kato, C., Kurose, Y., Sakamoto, M., Kato, S., Goto, T., Itoyama, Y., Aoki, M., and Nakagawara, A. (2004). NEDL1, a Novel Ubiquitin-protein Isopeptide Ligase for Dishevelled-1, Targets Mutant Superoxide Dismutase-1. *J. Biol. Chem.* 279, 11327–11335. <https://doi.org/10.1074/jbc.M312389200>.
- Shami Shah, A., Batrouni, A.G., Kim, D., Punyala, A., Cao, W., Han, C., Goldberg, M.L., Smolka, M.B., and Baskin, J.M. (2019). PLEKHA4/kramer Attenuates Dishevelled Ubiquitination to Modulate Wnt and Planar Cell Polarity Signaling. *Cell Rep.* 27, 2157–2170.e8. <https://doi.org/10.1016/j.celrep.2019.04.060>.
- Shami Shah, A., Cao, X., White, A.C., and Baskin, J.M. (2021). PLEKHA4 Promotes Wnt/ $\beta$ -catenin Signaling-Mediated G1/S Transition and Proliferation in Melanoma. *Cancer Res.* 81, 2029–2043. <https://doi.org/10.1158/0008-5472.CAN-20-2584>.
- Buchon, N., Broderick, N.A., Chakrabarti, S., and Lemaitre, B. (2009). Invasive and indigenous microbiota impact intestinal stem cell activity through multiple pathways in *Drosophila*. *Genes Dev.* 23, 2333–2344. <https://doi.org/10.1101/gad.1827009>.
- Marianes, A., and Spradling, A.C. (2013). Physiological and stem cell compartmentalization within the *Drosophila* midgut. *Elife* 2, e00886. <https://doi.org/10.7554/eLife.00886>.
- Buchon, N., Osman, D., David, F.P.A., Fang, H.Y., Boquete, J.-P., Deplancke, B., and Lemaitre, B. (2013). Morphological and Molecular Characterization of Adult Midgut Compartmentalization in *Drosophila*. *Cell Rep.* 3, 1725–1738. <https://doi.org/10.1016/j.celrep.2013.04.001>.
- Perochon, J., Carroll, L.R., and Cordero, J.B. (2018). Wnt Signaling in Intestinal Stem Cells: Lessons from Mice and Flies. *Genes* 9, 138. <https://doi.org/10.3390/genes9030138>.
- Hu, D.J.-K., Yun, J., Elstrott, J., and Jasper, H. (2021). Non-canonical Wnt signaling promotes directed migration of intestinal stem cells to sites of injury. *Nat. Commun.* 12, 7150. <https://doi.org/10.1038/s41467-021-27384-4>.
- Brunner, E., Peter, O., Schweizer, L., and Basler, K. (1997). pangolin encodes a Lef-1 homologue that acts downstream of Armadillo to transduce the Wingless signal in *Drosophila*. *Nature* 385, 829–833. <https://doi.org/10.1038/385829a0>.
- Chen, J., Xu, N., Wang, C., Huang, P., Huang, H., Jin, Z., Yu, Z., Cai, T., Jiao, R., and Xi, R. (2018). Transient Scute activation via a self-stimulatory loop directs enteroendocrine cell pair specification from self-renewing intestinal stem cells. *Nat. Cell Biol.* 20, 152–161. <https://doi.org/10.1038/s41556-017-0020-0>.
- Biteau, B., and Jasper, H. (2014). Slit/Robo signaling regulates cell fate decisions in the intestinal stem cell lineage of *Drosophila*. *Cell Rep.* 7, 1867–1875. <https://doi.org/10.1016/j.celrep.2014.05.024>.
- Micchelli, C.A., and Perrimon, N. (2006). Evidence that stem cells reside in the adult *Drosophila* midgut epithelium. *Nature* 439, 475–479. <https://doi.org/10.1038/nature04371>.
- Jiang, H., Grenley, M.O., Bravo, M.-J., Blumhagen, R.Z., and Edgar, B.A. (2011). EGFR/Ras/MAPK Signaling Mediates Adult Midgut Epithelial Homeostasis and Regeneration in *Drosophila*. *Cell Stem Cell* 8, 84–95. <https://doi.org/10.1016/j.stem.2010.11.026>.
- Brankatschk, M., and Eaton, S. (2010). Lipoprotein Particles Cross the Blood-Brain Barrier in *Drosophila*. *J. Neurosci.* 30, 10441–10447. <https://doi.org/10.1523/JNEUROSCI.5943-09.2010>.
- Schindelin, J., Arganda-Carreras, I., Frise, E., Kaynig, V., Longair, M., Pietzsch, T., Preibisch, S., Rueden, C., Saalfeld, S., Schmid, B., et al. (2012). Fiji: an open-source platform for biological-image analysis. *Nat. Methods* 9, 676–682. <https://doi.org/10.1038/nmeth.2019>.
- Tian, A., Benchabane, H., Wang, Z., and Ahmed, Y. (2016). Regulation of Stem Cell Proliferation and Cell Fate Specification by Wingless/Wnt Signaling Gradients Enriched at Adult Intestinal Compartment Boundaries. *PLoS Genet.* 12, e1005822. <https://doi.org/10.1371/journal.pgen.1005822>.
- Jiang, H., Patel, P.H., Kohlmaier, A., Grenley, M.O., McEwen, D.G., and Edgar, B.A. (2009). Cytokine/Jak/Stat Signaling Mediates Regeneration and Homeostasis in the *Drosophila* Midgut. *Cell* 137, 1343–1355. <https://doi.org/10.1016/j.cell.2009.05.014>.
- Cordero, J.B., Stefanatos, R.K., Scopelliti, A., Vidal, M., and Sansom, O.J. (2012). Inducible progenitor-derived Wingless regulates adult

- midgut regeneration in *Drosophila*. *EMBO J.* 31, 3901–3917. <https://doi.org/10.1038/emboj.2012.248>.
39. Wang, Z., Tian, A., Benchabane, H., Tacchelly-Benites, O., Yang, E., Nojima, H., and Ahmed, Y. (2016). The ADP-ribose polymerase Tankyrase regulates adult intestinal stem cell proliferation during homeostasis in *Drosophila*. *Development* 143, 1710–1720. <https://doi.org/10.1242/dev.127647>.
40. Gultekin, Y., and Steller, H. (2019). Axin proteolysis by Iduna is required for the regulation of stem cell proliferation and intestinal homeostasis in *Drosophila*. *Development* 146, dev169284. <https://doi.org/10.1242/dev.169284>.
41. Angers, S., Thorpe, C.J., Biechele, T.L., Goldenberg, S.J., Zheng, N., MacCoss, M.J., and Moon, R.T. (2006). The KLHL12–Cullin-3 ubiquitin ligase negatively regulates the Wnt– $\beta$ -catenin pathway by targeting Dishevelled for degradation. *Nat. Cell Biol.* 8, 348–357. <https://doi.org/10.1038/ncb1381>.
42. Strutt, H., Searle, E., Thomas-MacArthur, V., Brookfield, R., and Strutt, D. (2013). A Cul-3–BTB ubiquitylation pathway regulates junctional levels and asymmetry of core planar polarity proteins. *Development* 140, 1693–1702. <https://doi.org/10.1242/dev.089656>.

STAR★METHODS

KEY RESOURCES TABLE

REAGENT or RESOURCE	SOURCE	IDENTIFIER
<b>Antibodies</b>		
Anti-phosphoH3 (Mouse monoclonal)	Cell Signaling Technology	Cat#9706 RRID:AB_331748
Anti-Armadillo (Mouse monoclonal)	DSHB	Cat#N2 7A1 RRID:AB_528089
Anti-Prospero (Mouse monoclonal)	DSHB	Cat#MR1A RRID:AB_528440
Anti-Mouse Alexa Fluor 594 (Donkey)	Thermo Fisher Scientific	Cat#A21203 RRID:AB_141633
Anti-FLAG (M2)	Millipore Sigma	Cat#F1084 RRID:AB_262044
Anti-mCherry (1C51)	Millipore Sigma	Cat#MAB131873
Anti-HA	Roche	Cat#11867423001, RRID:AB_390918
Anti-GAPDH	Santa Cruz Biotechnology	Cat# sc-59540, RRID:AB_631587
Anti-Rabbit IgG-HRP	Jackson Immuno Research Labs	Cat# 111035144, RRID:AB_2307391
Anti-Mouse IgG-HRP	Jackson Immuno Research Labs	Cat# 115035146, RRID:AB_2307392
Anti-Rat IgG-HRP	Jackson Immuno Research Labs	Cat# 112-035-062, RRID:AB_2338133
<b>Bacterial and virus strains</b>		
<i>Erwinia carotovora carotovora</i> 15	Nicolas Buchon, Cornell University	N/A
<b>Chemicals, peptides, and recombinant proteins</b>		
Prolong Diamond antifade Mountant with DAPI	Thermo Fisher Scientific	Cat#P36971
16% paraformaldehyde	EMS	Cat# 15714
TRlzol	Life Technologies	Cat#15596018
PerfeCTa SYBR Green FastMix	Quantabio	Cat# 95055
<b>Experimental models: Cell lines</b>		
HEK 293T	Pietro De Camilli, Yale	N/A
<b>Experimental models: Organisms/strains</b>		
<i>D.melanogaster</i> : <i>W</i> <sup>1118</sup>	Bloomington Drosophila Stock Center	BDSC:3605 FLYB:FBst0003605 RRID:BDSC_3605
<i>D.melanogaster</i> : CantonS	Bloomington Drosophila Stock Center	BDSC:64349 FLYB:FBst0064349 RRID:BDSC_64349
<i>D.melanogaster</i> : <i>w</i> ; <i>da-Gal4</i> , <i>dipt RecA12;tub-Gal80<sup>ts</sup></i>	Buchon Nicolas, Cornell University	BDSC:12429 FLYB:FBal0121811 RRID:BDSC_12429
<i>D.melanogaster</i> : <i>y[1] sc[*] v[1] sev[21]; P[y[+t7.7] v[+t1.8]] = VALIUM20-mCherry. RNAi}attP2</i>	Bloomington Drosophila Stock Center	BDSC:35785 FLYB:FBst0035785 RRID:BDSC_35785

(Continued on next page)

**Continued**

REAGENT or RESOURCE	SOURCE	IDENTIFIER
<i>D.melanogaster</i> : <i>w<sup>-</sup></i> ; <i>esg-Gal4</i> ; UAS-GFP, <i>tub-Gal80<sup>ts</sup></i>	Micchelli et al. <sup>32</sup>	N/A
<i>D.melanogaster</i> : <i>w<sup>-</sup></i> ; <i>esg-Gal4</i> , UAS-eGFP; <i>Su(H)-Gal80</i> , <i>tub-Gal80<sup>ts</sup></i>	Hu et al. <sup>28</sup>	N/A
<i>D.melanogaster</i> : <i>w<sup>-</sup></i> ; <i>Su(H)-Gal4</i> ; UAS-GFP, <i>tub-Gal80<sup>ts</sup></i>	Dutta et al. <sup>12</sup>	N/A
<i>D.melanogaster</i> : <i>w<sup>-</sup></i> ; <i>myo1A-Gal4</i> ; UAS-GFP, <i>tub-Gal80<sup>ts</sup></i>	Buchon et al. <sup>4</sup>	N/A
<i>D.melanogaster</i> : <i>w<sup>-</sup></i> ; <i>pro-Gal4</i> ; UAS-GFP, <i>tub-Gal80<sup>ts</sup></i>	Dutta et al. <sup>12</sup>	N/A
<i>D.melanogaster</i> : <i>esg-Gal4</i> ; UAS-GFP, <i>tub-Gal80<sup>ts</sup></i> ; <i>Act&gt;STOP&gt;Gal4</i> , UAS- <i>flp</i>	Jiang et al. <sup>33</sup>	N/A
<i>D.melanogaster</i> : <i>w<sup>-</sup></i> ; <i>how-Gal4</i> ; UAS-GFP, <i>tub-Gal80<sup>ts</sup></i>	Dutta et al. <sup>12</sup>	N/A
<i>D.melanogaster</i> : <i>Lpp-Gal4</i> ; <i>Tub-Gal80<sup>ts</sup></i>	Brankatschk et al. <sup>34</sup>	N/A
<i>D.melanogaster</i> : <i>y[1] sc[*] v[1] sev[21]</i> ; P{y[+t7.7] v[+t1.8]} = TRiP.HMS03376)attP2	Bloomington Drosophila Stock Center	BDSC:51917 FLYB:FBst0051917 RRID:BDSC_51917
<i>D.melanogaster</i> : <i>y[1] sc[*] v[1] sev[21]</i> ; P{y[+t7.7] v[+t1.8]} = TRiP.HMC03751)attP40	Bloomington Drosophila Stock Center	BDSC:55612 FLYB:FBst0055612 RRID:BDSC_55612
<i>D.melanogaster</i> : <i>y[1] v[1]</i> ; P{y[+t7.7] v[+t1.8]} = TRiP.JF02306)attP2	Bloomington Drosophila Stock Center	BDSC:26743 FLYB:FBst0026743 RRID:BDSC_26743
<i>D.melanogaster</i> : <i>y[1] v[1]</i> ; P{y[+t7.7] v[+t1.8]} = TRiP.JF01796)attP2	Bloomington Drosophila Stock Center	BDSC:25790 FLYB:FBst0025790 RRID:BDSC_25790
<i>D.melanogaster</i> : <i>kmr<sup>1</sup></i>	Shami Shah et al. <sup>22</sup>	N/A
<i>D.melanogaster</i> : <i>kmr<sup>2</sup></i>	Shami Shah et al. <sup>22</sup>	N/A
<i>D.melanogaster</i> : <i>Sp/Cyow</i> ; <i>TM2/TM6B</i>	Chun Han, Cornell University	N/A
<i>D.melanogaster</i> : <i>fz3-RFP</i>	Tian et al. <sup>36</sup>	N/A
<b>Oligonucleotides</b>		
Fw primer (fly 3xFLAG Dsh cloning) CGC GAATTCAATGGACGCGGACAGGGG	This paper	N/A
Rv primer (fly 3xFLAG Dsh cloning) GAG GATCCCTACAATACGTAATTAATAC	This paper	N/A
Fw primer (fly mScarlet kelch cloning) TCG AATTCTATGATAGCTCTGAGTGCG	This paper	N/A
Rv primer (fly mScarlet kelch cloning) GTG GATCCTCACATGGGCTTGTCG	This paper	N/A
Rpl32 Fw: GACGCTTCAAGGGACAGTATCTG	Buchon et al. <sup>26</sup>	N/A
Rpl32 Rv: AAACGCGTTCTGCATGAG	Buchon et al. <sup>26</sup>	N/A
Kmr Fw: GGTGGAACATCGAGCAGTTCA	This paper	N/A
Kmr Rv: CGCCAGATACGTTGCTCC	This paper	N/A
Kel Fw: TTGACGACACTGAGTCCACG	This paper	N/A
Kel Rv: TGTGCGGTAAAGTGGCTCAT	This paper	N/A
Wg Fw: CCAACCCACGAAGTACAGA	This paper	N/A
Wg Rv: CATGGATGGGGTGGTTAAG	This paper	N/A

(Continued on next page)

**Continued**

REAGENT or RESOURCE	SOURCE	IDENTIFIER
Fz3 Fw: TCTGGGACCGAACTAGATGGA	This paper	N/A
Fz3 Rv: CACGAGCGGAGCAAAGTAT	This paper	N/A
Naked Fw: CGGGCATCACGGCAAGATAA	This paper	N/A
Naked Rv: GAGGCGCACGTTGATTGTC	This paper	N/A
Notum Fw: ATTGAGGGACACCAGCATGAA	This paper	N/A
Notum Rv: CGCAGATAGAAACCGGCATGA	This paper	N/A
Upd2 Fw: TTCTCCGGCAAATCAGAGATCC	Wang et al. <sup>39</sup>	N/A
Upd2 Rv: GCGCTTGATAACTCGTCCTTG	Wang et al. <sup>39</sup>	N/A
Upd3 Fw: AGCCGGAGCGGTAACAAAA	Wang et al. <sup>39</sup>	N/A
Upd3 Rv: CGAGTAAGATCAGTGACCAGTTC	Wang et al. <sup>39</sup>	N/A

**Recombinant DNA**

pEGFP-C1	Clontech	Cat#6084-1
mScarlet-i	This paper	N/A
HA-Ub	Pietro De Camilli, Yale	N/A
pCMV-3xFLAG	Sigma	Cat#E7658

**Software and algorithms**

ImageJ	NIH	N/A
Zen Blue 2.3	Zeiss	N/A
Image Lab Software	Bio-Rad	N/A

**RESOURCE AVAILABILITY****Lead contact**

Further information and requests for resources and reagents should be directed to and will be fulfilled by the lead contact, Jeremy M. Baskin ([jeremy.baskin@cornell.edu](mailto:jeremy.baskin@cornell.edu)).

**Materials availability**

This study did not generate new unique reagents.

**Data and code availability**

- Data: Data reported in this paper will be shared by the [lead contact](#) upon request.
- Code: This paper does not report original code.
- All other requests: Any additional information required to reanalyze the data reported will be shared by the [lead contact](#) upon request.

**EXPERIMENTAL MODEL AND STUDY PARTICIPANT DETAILS****Fly stock generation and husbandry**

Flies were maintained at room temperature in standard yeast glucose medium (50 g/L yeast, 60 g/L yellow cornmeal, 40 g/L sucrose, 7 g/L fly agar, 26.5 mL/L moldex, 12 mL/L acid mix). Fly stocks used in this study include: *w*<sup>1118</sup> and *CantonS*; *Gal4* drivers used were '*w*'; *esg-Gal4*; *UAS-GFP*, *tub-Gal80<sup>ts</sup>* (*esg<sup>ts</sup>*, progenitor-specific);<sup>32</sup> '*w*<sup>-</sup>'; *esg-Gal4*, *UAS-eGFP*; *Su(H)-Gal80*, *tub-Gal80<sup>ts</sup>* (*esg::Su(H)<sup>ts</sup>*, ISC-specific); '*w*<sup>-</sup>'; *Su(H)-Gal4*; *UAS-GFP*, *tub-Gal80<sup>ts</sup>* (*Su(H)<sup>ts</sup>*, EB-specific); '*w*<sup>-</sup>'; *myo1A-Gal4*; *UAS-GFP*, *tub-Gal80<sup>ts</sup>*' (*myo<sup>ts</sup>*, EC-specific)<sup>4</sup>; '*w*<sup>-</sup>'; *pro-Gal4*; *UAS-GFP*, *tub-Gal80<sup>ts</sup>*' (*pro<sup>ts</sup>*, EE-specific);<sup>12</sup> '*esg-Gal4*; *UAS-GFP*, *tub-Gal80<sup>ts</sup>*'; *Act>STOP>Gal4*, *UAS-flp*' (*Esg<sup>ts</sup>* F/O, progenitors<sup>+</sup> marked lineage);<sup>33</sup> '*w*<sup>-</sup>'; *how-Gal4*; *UAS-GFP*, *tub-Gal80<sup>ts</sup>* (*how<sup>ts</sup>*, visceral muscle-specific); *tub-Gal80<sup>ts</sup>*, *UAS-GFP*; *lpp-Gal4* (*lpp<sup>ts</sup>*, fat body-specific);<sup>34</sup> '*w*<sup>-</sup>'; *da-Gal4*, *tub-Gal80<sup>ts</sup>* (*da<sup>ts</sup>*, whole body) (BDSC, 12429); *UAS-mCherry* RNAi (BDSC:35785); *UAS-kmr* RNAi (BDSC, 51917); *UAS-kelch* RNAi (BDSC, 55612); *UAS-pan* RNAi (BDSC, 26743); *UAS-OTK* RNAi (BDSC, 25790); *fz3-RFP* (obtained from Yashi Ahmed).<sup>36</sup> Knockout strains *kmr*<sup>1</sup> and *kmr*<sup>2</sup> were generated with CRISPR/Cas9 gene deletion by our lab.<sup>22</sup> Strains *sp/cyow*; *TM2/TM6B* (obtained from Chun Han) were used to cross with *kmr*<sup>1</sup>, *kmr*<sup>2</sup>, *kmr* RNAi and/or *kelch* RNAi separately, then back crossed with cell type specific *Gal4* system. See [key resources table](#) for details.

### Mammalian cell culture

HEK 293T cells were grown in Dulbecco's Modified Eagle Medium (DMEM) supplemented with FBS (10%), P/S (1%), and sodium pyruvate (1 mM) at 37°C in a 5% CO<sub>2</sub> atmosphere. The cell line was obtained from ATCC, used without further authentication, and confirmed to be negative for mycoplasma.

## METHOD DETAILS

### Infection of flies with *Ecc15*

Flies were maintained at room temperature or at 18°C in a 12 h light/12 h dark cycle incubator. Only posterior midguts of female flies were analyzed in this study, except that pH3<sup>+</sup> cells were quantified from the whole midguts. CantonS, a wildtype inbred line, was used as the wild-type control for all experiments unless otherwise indicated. Experiments using *kramer* mutants, which used *w<sup>1118</sup>* as control. F1 developing progenies of crosses involving the temperature-sensitive (*Gal4-Gal80<sup>ts</sup>*) system were maintained at 18°C, and adults were collected on the 5th day after eclosion, to allow for proper midgut development. F1 progenies were then transferred to 29°C for 6 days to allow for transgene induction to take effect. F1 flies were then transferred to empty vials for a 2 h starvation, followed by 12–16 h *Ecc15* infection at 29°C.<sup>1</sup> *Ecc15* was cultured in 500 mL of LB medium for 16 h at 30°C. The culture was pelleted, resuspended in water to an OD<sub>600</sub> of 200. Then *Ecc15* was diluted with the same volume of sucrose (1:4 ratio of 25% sucrose:water) to OD<sub>100</sub> in a 2.5% sucrose solution. Then, 150 μL of diluted *Ecc15* culture was deposited on a Whatman filter paper, which was inserted into the food vial and placed on top of the food. In the *Ecc15* infection experiments, 2.5% sucrose was used as unchallenged control. Whole guts were dissected from *Ecc15*-infected and control flies for further analyses.

### Immunohistochemistry and histology

The immunohistochemistry protocol was adapted from a previous study.<sup>5</sup> Immunostaining was performed at room temperature. *Drosophila* midguts were dissected in 1X PBS. Dissected midguts were fixed in 4% paraformaldehyde (Electron Microscopy Sciences, Hatfield, PA, Cat# 15714) for 60–90 min and subsequently washed three times with 0.1% Triton X-100 (Cat# IB07100, IBI Scientific, Dubuque, IA) that was diluted in 1X PBS. Fixed midguts were blocked for 1 h in blocking solution (1% bovine serum albumin, Cat# A8806, Sigma-Aldrich, St. Louis, MO; 1% normal donkey serum, Cat# 102644-006, VWR, Radnor, PA. in PBS). Then the primary antibody (1:1000) was added into the blocking solution with midguts and incubated overnight. The primary antibodies used were mouse anti-pH3 (1:500, Cat# 9706S, Cell Signaling Technology, Danvers, MA), mouse anti-Armadillo (1:10, Cat# N2 7A1, DSHB), and mouse anti-Prospero (1:100, Cat# MR1A, DSHB). After three washes with 0.1% Triton X-100 in PBS, the midguts were incubated with secondary antibody (donkey anti-mouse Alexa 594 (1:400, Cat# A21203, Thermo Fisher)) for 2 h in blocking solution. Midguts were then washed three times in 1X PBS. DNA was then stained with DAPI and midguts were mounted with ProLong Diamond Antifade Mountant (Cat# P36971, Thermo Fisher) overnight. Imaging was performed on a Zeiss LSM 800 confocal laser scanning microscope equipped with EC Plan-Neofluar 10X 0.3 NA and Plan-Apochromat 20×0.8 NA air objectives, Plan Apochromat 40X 1.4 NA and Plan-Apochromat 63X 1.4 NA f/ELYRA oil immersion objectives, 405, 488, 561, and 640 nm solid-state lasers, two GaAsP PMT detectors, and an Airyscan module (Carl Zeiss Microscopy, Thornwood, NY). Images were acquired using Zeiss Zen Blue 2.3 and analyzed using ImageJ/FIJI.<sup>35</sup> pH3<sup>+</sup> cells were counted directly in epifluorescence mode using a 20X objective lens. Armadillo<sup>+</sup>/Prospero<sup>-</sup> labeled progenitor cells and Prospero<sup>+</sup> cells were counted manually within a field of vision of posterior midguts.

### qRT-PCR

Fifteen midguts of each genotype were dissected in PBS on ice, and RNA was extracted using Trizol. Samples were centrifuged, supernatant was discarded, and 1 mL of Trizol was added to the midgut pellet, which was stored at –80°C. The Trizol solution was thawed at room temperature and 200 μL chloroform was added. The tubes were vortexed for 15 s and placed on ice for 15 min. The samples were centrifuged cold for 15 min at 13000 × g. The upper aqueous phase was transferred to a new tube, and 500 μL isopropanol was added. The tubes were vortexed for 15 s and placed at room temperature for 10 min. The samples were then centrifuged at 4°C for 10 min at 12,000 × g. The supernatant was removed, and 750 μL of 75% ethanol was added. The samples were centrifuged at 7500 × g for 5 min at 4°C, and the supernatant was discarded. The RNA pellet was air dried for 2 min in a fume hood, and 8 μL of RNase-free water was added. cDNA synthesis was performed by mixing RNA (1 μg) with 1 μL oligodT (TTTTTTTTTTTTTTTTTTTT, dissolved at 500 μg/mL in water), and the mixture was heated to 70°C for 3 min and then cooled on ice. 4 μL of 5X 1<sup>st</sup> strand buffer, 2 μL DTT (100 mM), 0.8 μL dNTP mix (25 mM), and 0.5 μL MMLV reverse transcriptase (Takara Bio) were added to the RNA mixture, and RNase-free water was added up to 20 μL. The reaction was incubated at 42°C for 1 h and then 70°C for 15 min. Finally, the reaction was diluted to 100 μL with RNase-free water. qRT-PCR was performed in biological and technical triplicate using PerfeCTa SYBR Green FastMix (Cat# 95055, Quantabio) on Roche LightCycler 480. Data analysis was performed using the delta delta Cp method and using GAPDH as a control.

### Plasmids and cloning

Total RNA was extracted from 10 adult *Drosophila w<sup>1118</sup>* flies. 1 μg of this RNA was used as the template for cDNA synthesis. PCR amplification of *dsh* and *kel* cDNA was performed using specific primers:

Dsh-Forward: CGCGAATTCAATGGACGCGGACAGGGG.

Dsh-Reverse: GAGGATCCCTACAATACGTAATTAATAC.

Kel-Forward: TCGAATTCTATGATAGCTCTGAGTGCG.

Kel-Reverse: GTGGATCCTCACATGGGCTTGTCG.

The amplified cDNAs for *dsh* and *kel* were cloned into pCMV-3xFLAG and mScarlet-i-C1 (mSc-i-C1) vectors, respectively. Both constructs used EcoRI and BamHI restriction sites to facilitate the generation of 3xFLAG-Dsh and mSc-i-Kel constructs.

### Transfection of HEK 293T cells

HEK 293T cells were transfected 16–20 h after seeding to 60 mm dishes at 40% confluency using Lipofectamine 2000 following the manufacturer's protocol. In brief, for each dish, a combination of plasmids (listed below, optimized to ensure equal expression of Dsh and Kel constructs across multiple samples) and Lipofectamine 2000 (6  $\mu$ L) were diluted respectively in 300  $\mu$ L serum-free DMEM and then mixed. The resulting mixture was incubated at room temperature for 20 min before being added to the cells in DMEM supplemented with FBS, P/S, and sodium pyruvate (1 mM). 6 h after transfection, the DNA-containing medium was replaced with fresh growth medium. Lysis and downstream analysis were performed at least 24 h after transfection.

Plasmids used for co-transfection:

Combination A: 3xFLAG-Dsh (2  $\mu$ g), mSc-i-Kelch (2  $\mu$ g), and HA-Ub (2  $\mu$ g);

Combination B: 3xFLAG-Dsh (2  $\mu$ g), mSc-i-C1 (1  $\mu$ g), and HA-Ub (2  $\mu$ g);

Combination C: 3xFLAG-C1 (1  $\mu$ g), mSc-i-Kelch (2  $\mu$ g), and HA-Ub (2  $\mu$ g).

### Cell lysis and preparation of whole cell lysates for SDS-PAGE

A 60 mm dish of HEK 293T cells transfected as above was rinsed with PBS for three times, and ice-cold RIPA lysis buffer (pH 8.0; 250  $\mu$ L) supplemented with 1 $\times$  cOmplete protease inhibitor cocktail (Roche) was added. Cell monolayers were scraped off from the dish, and the collected lysate was homogenized by sonication (20% amplitude; 4 s) and centrifuged (13000  $\times$  g; 10 min) at 4°C. The bicinchoninic acid (BCA) assay was performed with Pierce BCA Protein Assay Kits (Thermo) to determine the protein concentration in the clarified lysate. 200  $\mu$ g of lysate was removed and diluted with 6 $\times$  SDS buffer (16.7  $\mu$ L) and water to a final volume of 100  $\mu$ L. The resultant sample was heated to 95°C for 5 min and stored at –20°C until analysis by SDS-PAGE along with the corresponding immunoprecipitation sample prepared as described below.

### Immunoprecipitation

ANTI-FLAG M2 Affinity Gel (Millipore Sigma) was washed with RIPA buffer (pH 8.0) three times. The washed affinity gel (20  $\mu$ L) was mixed with 2 mg of the clarified lysate in an Eppendorf tube. Ice-cold RIPA buffer (pH 8.0) supplemented with 1 $\times$  cOmplete protease inhibitor cocktail was added to dilute the suspension to 1.5 mL. The suspension was gently spun at 4°C for 2 h. The affinity gel was centrifuged (1000  $\times$  g; 1 min), and the supernatant was carefully removed. The gel pellet was rinsed with 1 mL ice-cold RIPA buffer (pH 8.0) for three times. Finally, the affinity gel was resuspended in 80  $\mu$ L 1.5 $\times$  SDS buffer and heated to 95°C for 5 min and cooled down to ambient temperature. The resulting immunoprecipitation sample was used in SDS-PAGE immediately.

### SDS-PAGE and Western blotting

Samples of whole cell lysate and immunoprecipitation were analyzed by SDS-PAGE using 7%, 9%, and 12% acrylamide. The separated proteins were transferred to nitrocellulose by the wet transfer method and blocked in 5% fat-free skimmed milk in 1 $\times$  TBS-T (blocking buffer) for 1 h at ambient temperature. Subsequently, primary antibodies (manufacturer and dilution were listed in the table below) were added directly to the blocking buffer and allowed to stain the membrane at 4°C for 12–16 h. Following three 7-min rinses with TBS-T, secondary antibody staining was performed for 1 h at ambient temperature. Membranes were rinsed three times in TBS-T for 7 min each and then in TBS for 7 min twice. Finally, the membranes were developed by using either Clarity or Clarity Max ECL Western blotting substrate (Bio-Rad) for 5 min and visualized using a ChemiDoc MP Imaging System (Bio-Rad). Data analysis was performed using the Image Lab software (Bio-Rad).

## QUANTIFICATION AND STATISTICAL ANALYSIS

### Statistical analysis

All plots were generated using GraphPad Prism v.7.0 (<https://www.graphpad.com>). Statistical significance between different treatments were assessed using one-way ANOVA followed by Tukey's post-hoc test. Sample number (n), error bars, and asterisks to denote *p* values are defined contextually within individual figure legends.